Title

Gut enterochromaffin cells drive visceral pain and anxiety

Journal

Nature, 616(7955)

ISSN

0028-0836

Authors

Bayrer, James R
Castro, Joel
Venkataraman, Archana
et al.

Publication Date

2023-04-06

DOI

10.1038/s41586-023-05829-8

Peer reviewed

Published in final edited form as:

Nature. 2023 April ; 616(7955): 137–142. doi:10.1038/s41586-023-05829-8.

Gut Enterochromaffin Cells Drive Visceral Pain and Anxiety

James R. Bayrer[1,7,*], **Joel Castro**[2,3,*], **Archana Venkataraman**[4], **Kouki K. Touhara**[5], **Nathan D. Rossen**[5,6], **Ryan D. Morrie**[5,#], **Jessica Maddern**[2,3], **Aenea Hendry**[2,3], **Kristina N. Braverman**[1,#], **Sonia Garcia-Caraballo**[2,3], **Gudrun Schober**[2,3], **Mariana Brizuela**[2,3], **Fernanda M. Castro Navarro**[4], **Carla Bueno-Silva**[1], **Holly A. Ingraham**[4,7], **Stuart M. Brierley**[2,3,7], **David Julius**[5,7]

[1]Department of Pediatrics, University of California, San Francisco, San Francisco, CA USA

[2]College of Medicine and Public Health, Flinders Health and Medical Research Institute, Adelaide, SA 5042, AUSTRALIA

[3]Hopwood Centre for Neurobiology, Lifelong Health, South Australian Health and Medical Research Institute (SAHMRI), North Terrace, Adelaide, SA 5000, AUSTRALIA

[4]Department of Cellular and Molecular Pharmacology, University of California, San Francisco, CA USA

[5]Department of Physiology, University of California, San Francisco, CA USA

[6]Tetrad Graduate Program, University of California, San Francisco, CA USA

Abstract

Gastrointestinal (GI) discomfort is a hallmark of most gut disorders and represents a significant component of chronic visceral pain[1]. For the growing population afflicted by irritable bowel syndrome (IBS), GI hypersensitivity and pain persist long after tissue injury has resolved[2]. IBS also exhibits a strong sex bias afflicting women three-fold more than men[1]. Here, we focus on enterochromaffin (EC) cells, which are rare excitable, serotonergic neuroendocrine cells within the gut epithelium[3–5]. EC cells detect and transduce noxious stimuli to nearby mucosal nerve endings[3,6], but involvement of this signaling pathway in visceral pain and attendant sex differences

7 Corresponding Authors: david.julius@ucsf.edu, stuart.brierley@flinders.edu.au, holly.ingraham@ucsf.edu, james.bayrer@ucsf.edu.

* Equal Contribution

[#]Present address:

Maze Therapeutics, 171 Oyster Point Blvd, South San Francisco, CA USA (R.D.M.)

Jansen, Johnson & Johnson, 3210 Merryfield Row, San Diego, CA USA (K.N.B.)

AUTHOR CONTRIBUTIONS

R.D. M. developed and implemented transgenic strategies for targeting DREADD and PfTox expression to EC cells. N.D.R., A.V. and R.D.M. characterized DREADD and PfTox expression in these lines histologically. J.C. and S.M.B. designed, performed, and analyzed *ex vivo* studies mechanically and optogenetically stimulating colonic mucosal afferents. M.B. and S.M.B. designed, performed, and analyzed *ex vivo* studies on colonic distension-sensitive afferents. M.B performed and analyzed *in vitro* responses of Na$_V$1.8-GCaMP6 DRG neurons. G.S., J.M., J.C., S.M.B, K.B., and J.R.B. designed, performed, and analyzed visceromotor response to colorectal distension. J.C., A.H., and S.M.B. designed, performed, and analyzed intravital GCaMP imaging studies. S.G-C. quantified eYFP expression in male and female Na$_V$1.8-Ch2 DRG neurons. K.K.T. quantified serotonin release from organoids. A.V., F.C.N ad C.B.S. collected blood samples and measured serotonin levels in serum. A.V. performed and analyzed experiments to assess anxiety-related behaviors. H.A.I., J.R.B., S.M.B., and D.J. wrote the manuscript with input and suggestions from all authors and provided advice and guidance throughout.

COMPETING INTERESTS

The authors declare no competing interests.

has not been assessed. By enhancing or suppressing EC cell function *in vivo*, we show that these cells are sufficient to elicit hypersensitivity to gut distension and necessary for the sensitizing actions of isovalerate, a bacterial short-chain fatty acid associated with GI inflammation[7,8]. Remarkably, prolonged EC cell activation produced persistent visceral hypersensitivity, even in the absence of an instigating inflammatory episode. Furthermore, perturbing EC cell activity promoted anxiety-like behaviors that normalized after blocking serotonergic signaling. Sex differences were noted across a range of paradigms, indicating that the EC cell-mucosal afferent circuit is tonically engaged in females. Our findings validate a critical role for EC cell-mucosal afferent signaling in acute and persistent GI pain while highlighting genetic models for studying visceral hypersensitivity and the sex bias of gut pain.

Keywords

Visceral Pain; Gut-Brain Axis; Nociception; Mucosal Afferents; Enterochromaffin Cells; Irritable Bowel Syndrome (IBS); Anxiety-Like Behavior; Sex-Differences

The gut is lined by a thin epithelial sheet containing rare, but functionally diverse enteroendocrine cells that release hormones and neurotransmitters to regulate nutrient absorption, digestion, motility, feeding behaviors, and sensory perception[9–12]. Enterochromaffin (EC) cells, a unique subtype of enteroendocrine cells, detect environmental and endogenous stimuli capable of eliciting or exacerbating pain, including dietary irritants, microbial metabolites, inflammatory agents, mechanical distension, and stress-associated hormones and neurotransmitters[3,6,13,14]. Once activated, EC cells release serotonin onto nearby 5-HT_3 receptor-expressing sensory nerve endings that transmit nociceptive signals to the spinal cord[3,14,15]. Sensory nerve endings themselves detect noxious stimuli[16,17] and distinct types of spinal afferents innervate the gut, including stretch-insensitive mucosal fibers and those that innervate muscular, vascular, or mesenteric compartments and respond to distension over a range of thresholds[2]. Thus, it remains to be established whether and to what extent EC cells and neighboring mucosal afferents contribute to acute and/or persistent visceral pain and attendant sex differences. Here, we address these issues by silencing or ectopically activating EC cells in mice and assessing consequences regarding colonic sensory nerve fiber activity, visceral sensitivity, and behavior. Our results implicate EC cells and mucosal afferents as critical initiators of visceral pain and anxiety associated with IBS or other inflammatory or post-inflammatory GI disorders.

EC cells promote gut hypersensitivity

Bacterially derived short-chain fatty acids are known activators of enteroendocrine cells[3,7,18]. Some, such as isovalerate, are elevated in individuals with visceral hypersensitivity and may contribute to enhanced pain sensation[8,19]. We have previously shown that isovalerate activates EC cells via the G protein-coupled receptor Olfr558, producing serotonin-dependent mechanical sensitization of primary afferents in an *ex vivo* nerve-gut model[3]. Because both EC cells and sensory nerve fibers are mechanically responsive[20–22], we wondered whether isovalerate sensitizes nerve fibers to other non-

mechanical stimuli. We therefore used optogenetics to activate $Na_V1.8$-positive sensory neurons[23], which constitute > 95% of colon-innervating spinal afferents. Indeed, application of isovalerate to *ex vivo* nerve-gut preparations from $Na_V1.8$-ChR2 male mice boosted sensitivity of mucosal afferents to light (Fig. 1a, b, Extended Data Fig. 1a–c, and Extended Data Table 1). Remarkably, fibers from females showed greatly elevated baseline responses, even at the lowest light intensity, with no further enhancement by isovalerate (Fig. 1c, Extended Data Fig. 1b–c). Thus isovalerate-mediated sensitization is not specific to mechanical stimulation of EC cells or sensory neurons, but more broadly enhances excitability of this circuit. in a sexually dimorphic manner. Importantly there was no difference in channelrhodopsin-eYFP expression in dorsal root ganglia (DRG) from female and male $Na_V1.8$-ChR2 mice (Extended Data Fig. 1d).

Intravital calcium imaging of DRG[24] in $Na_V1.8$-GCaMP6s mice allowed us to determine how many neurons display baseline activity and were sensitized by intracolonic delivery of isovalerate *in vivo* (Fig. 1d). Here again, we noticed that basal neuronal activity within lumbosacral ganglia was substantially higher in females (Fig. 1e–h), suggesting enhanced activity of neurons that innervate visceral target organs including the colon. In males, 6.5% of neurons were activated by intracolonic isovalerate, while in females, far fewer cells (2.2%) were isovalerate sensitive (Fig. 1e–i). Isovalerate responses in males were attenuated by co-administration of the selective 5-HT_3 receptor antagonist, alosetron (Fig. 1i, Extended Data Fig. 1e), consistent with a mechanism in which isovalerate elicits release of serotonin from EC cells followed by activation of 5-HT_3 receptors on nearby sensory nerve endings. Alosetron did not alter the percentage of isovalerate sensitive neurons in females (Fig. 1i). There was no difference in the responsiveness of DRG neurons from female and male $Na_V1.8$-GCaMP6s mice to a variety of chemical stimuli, indicating that expression of GCaMP6s and neuronal excitability are comparable across sexes (Extended Data Fig. 1f).

To determine whether isovalerate enhances pain-related behavior, we measured reflex motor responses to colorectal distension in the presence or absence of intracolonically delivered isovalerate (Fig. 1j). Indeed, isovalerate produced substantial enhancement of this visceromotor response (VMR) across a range of distension pressures in males, whether measured within the same animal (Fig. 1k and Extended Data Fig. 1g) or across cohorts (Extended Data Fig. 1h). This behavioral effect was severely blunted in females, perhaps reflecting a narrower dynamic range (Fig. 1l and Extended Data Fig. 1g, 1h) and in keeping with the higher cellular baseline activity noted above. Importantly, colonic compliance was the same irrespective of sex or treatment (Extended Data Fig. 1i).

To ask if the sensitizing effect of isovalerate was mediated specifically by EC cells, we exploited the ability of tetanus toxin (TeNT) to inhibit synaptic vesicle fusion and neurotransmitter release from excitable cells[25]. We employed an intersectional genetic approach to target expression of TeNT (or DREADD receptors, see below) to EC cells. Briefly, a *Pet1Flp* allele favoring recombination in gut enteroendocrine cells was used in conjunction with a *Tac1Cre* driver that limits recombination to tachykinin-expressing cells (Fig. 2a). Indeed, within the gut our *Pet1Flp*;*Tac1Cre* line selectively targets EC cells (Fig. 2b) with no evidence of transgenic marker expression in serotonergic raphe nuclei, spinal cord, DRG sensory ganglia, or other enteroendocrine cell subtypes, highlighting

the remarkably small number of intestinal cells targeted and controlled by this genetic manipulation. Expression of TeNT or DREADD receptor did not alter the prevalence of EC cells (Extended Data Fig. 2). We also generated a *Vil1Cre-Pet1Flp* line that limits recombination predominantly to EC cells (Fig. 2a,b and Extended Data Fig. 2g), and these mice were used in one set of *ex vivo* studies (see below).

To validate a functional effect of TeNT expression, we measured stimulus-evoked serotonin release using intestinal organoids derived from TeNT-expressing animals (EC^{PFTtox}). The electrophilic irritant, allyl isothiocyanate (AITC), was used to activate native TRPA1 channels on EC cells and stimulate serotonin release. We observed a substantial (~30%) diminution in AITC-evoked serotonin release from EC^{PFTox} compared to Tac^{Cre} control organoids (Fig. 2c). Transmitter levels were similarly decreased in serum from EC^{PFTox} mice (Fig. 2c), reflecting the role of EC cells as a primary source of peripheral serotonin[26,27].

Whereas application of isovalerate to *ex vivo* gut-nerve preparations from Tac^{Cre} control animals enhanced responses of sensory nerves to mechanical stimulation of the mucosa, especially in males (Fig. 2d and Extended Data Fig. 3a–c), no such sensitization was observed with preparations from male or female EC^{PFTox} mice (Fig. 2d and Extended Data Fig. 3a–c). These findings confirm that the sensitizing effects of isovalerate are mediated via EC cells. Furthermore, baseline VMRs were diminished in EC^{PFTox} mice versus control littermates (Fig. 2e,f and Extended Data Fig. 3d), especially in females. Consistent with the *ex vivo* results, the robust sensitizing effect of intracolonic isovalerate on distension evoked VMR in males was abrogated in EC^{PFTox} mice (Fig. 2g). Taken together, these results show that EC cells contribute substantially to visceral nociception. Moreover, silencing EC cells has a proportionally greater effect in females, whereas males show greater isovalerate-evoked sensitization. These observations are consistent with the concept that the EC cell-nociceptor circuit in females is tonically engaged and thus exhibits a narrower dynamic range compared to males.

Sex-dependent visceral hypersensitivity

We next used chemogenetics to ask if EC cell activation is sufficient to generate visceral hypersensitivity. Using the same transgenic strategy described above, an activating DREADD receptor (hM3Dq) was expressed in EC cells to enable their selective pharmacological activation by deschloroclozapine (DCZ) or clozapine N-oxide (CNO) (Fig. 3a,b and Extended Data Fig. 2b–g). Applying a DREADD agonist to intestinal organoids derived from these EC^{hM3Dq} mice promoted EC cell activation and serotonin release (Fig. 3c and Extended Data Fig. 4a). A similar increase in serum serotonin content was seen in EC^{hM3Dq} females (but not males) at 15 minutes post-DCZ treatment, subsiding by 30 min. (Fig. 3c).

Application of DREADD agonists rendered fibers from EC^{hM3Dq} animals hypersensitive to mucosal mechanical stimulation without affecting those from Tac^{Cre} controls (Fig. 3d and Extended Data Fig. 4b–d), and this sensitization was more pronounced in males. To examine visceral hypersensitivity *in vivo*, we administered a DREADD agonist to EC^{hM3Dq} mice 15

min prior to colorectal distension, in which case we observed a significant increase in the VMR across a range of colonic pressures for males, with a trend towards significance in females (Fig. 3e and Extended Data Fig. 4e). Consistent with our intravital DRG results (Fig 1e,i), administration of alosetron blocked DCZ-mediated enhancement of the VMR in males (Fig. 3f). No difference in colonic compliance was evident between Tac^{Cre} and EC^{hM3Dq} mice (Extended Data Fig. 4f). Overall, these sex differences are consistent with the notion that the EC cell-mucosal afferent circuit exerts a higher tonic contribution to colonic sensitivity in females with a consequently smaller window for enhancement.

Persistent visceral hypersensitivity

Our results thus far show that stimulation of EC cells is sufficient to elicit acute visceral hypersensitivity, but can prolonged activation produce persistent sensitization resembling that observed in IBS? To address this question, we treated mice with DCZ daily for three weeks and assessed the VMR to colonic distension at 72 hours after cessation of agonist treatment (Fig. 3g). Remarkably, EC^{hM3Dq} animals maintained heightened sensitivity compared with controls following this drug washout period, demonstrating that EC cell activation is sufficient to drive both acute and persistent visceral pain (Fig. 3h, i). A more extensive temporal analysis will determine whether this ‘colitis-free’ sensitization paradigm represents a *bona fide* chronic (long-term) pain model.

Considering previous studies suggesting a role for EC cell-mediated serotonin release in regulating gut motility[13,15], we examined relevant parameters in EC^{hM3Dq} and EC^{PFTox} mice, including whole GI and colonic transit times. No significant differences were observed in these tests (Extended Data Fig. 5), highlighting the specificity of the pain phenotypes observed with these transgenic models.

Mucosal fibers convey EC cell signals

Primary afferent nerve fibers terminate in distinct layers of the gut, including mucosal, muscular, and vascular compartments, as well as the mesentery (Fig. 4a)[28]. It has generally been assumed that nerve fibers with low and high thresholds to distension drive visceral pain, rather than distension-insensitive mucosal afferents, which are instead exquisitely sensitive to small deformations of the mucosa[22]. However, given the observed necessity of EC cells in mediating this pain response, we asked whether fibers other than those innervating the mucosa are impacted by EC cell activation. To address this question, we used a modified *ex vivo* nerve-gut model in which pressurization of an intact colonic loop activates spiking in distension-sensitive afferents (including low and high threshold and wide dynamic range fibers) that detect circumferential tension applied across their receptive fields[29]. Nerves innervating the mucosal layer do not respond in this paradigm, allowing us to distinguish them from these other afferent types. These recordings were performed with mice in which EC cell-selective expression of TeNT or DREADD receptor was directed by *Pet1Flp;Vil1Cre* recombination.

In control mice, application of isovalerate failed to enhance activation of distension-sensitive afferents that innervate the non-mucosal layers (Extended Data Fig. 6). As expected,

preparations from EC^{PFTox} female or male mice, which showed diminished VMRs to colorectal distension, exhibited normal distension-sensitive nerve fiber activation before or after treatment with isovalerate (Fig. 4b). The same was true for preparations from EC^{hM3Dq} female and male mice, where CNO treatment had no effect on distension-sensitive fibers (Fig. 4c). Taken together, these results suggest that modulation of visceral pain is driven by distension-insensitive mucosal afferents that are instead responsive to local tissue deformation and interact directly with EC cells in the mucosal layer.

EC cell activity modulates anxiety

Functional GI disorders are often associated with increased anxiety as a manifestation of complex pain or sensory processing disorders that might affect bidirectional gut-brain signaling[1]. We therefore asked if chronic activation or suppression of EC cells influences anxiety states by assessing behavior in a standard elevated plus maze paradigm. We found that naive EC^{hM3Dq} animals treated with DCZ spent less time in the open arms (although total movement parameters in the closed arms did not differ), indicative of increased anxiety (Fig. 5 and Extended Data Fig. 7a). Importantly, co-administration of alosetron reversed the effects of DCZ (Fig. 5a). Taken together, these results support a role for serotonergic EC cell-mucosal afferent signaling in modulating both nociceptive and affective components of disordered gut-brain communication, although other effects of EC cell-released serotonin or other transmitters cannot be excluded. Interestingly, EC^{PFTox} animals also spent less time in the open arms (Fig. 5b and Extended Data Fig. 7b), suggesting that perturbing GI function through chronic suppression of EC cell activity is similarly anxiogenic. This was further substantiated by a significant change in the marble-burying assay, whereas no differences were observed in nestlet building or conditional fear behavior (Extended Data Fig. 7c–e).

DISCUSSION

Recent studies suggest that mediators released from the colonic epithelium elicit or inhibit visceral pain[30–32]. We now show that visceral pain and anxiety can be driven by an exceedingly small subpopulation of enteroendocrine cells, the EC cells, and their interaction with mucosal afferents. This is remarkable as mucosal afferents, which respond only to the smallest of stimuli deforming the mucosa, have not previously been considered key drivers of visceral pain, even though they show heightened responses in models of chronic visceral hypersensitivity. This role has historically been considered the domain of low threshold[33], wide dynamic range[33], or high threshold[2,16,34] distension-sensitive afferents, which are polymodal and respond to a wide variety of inflammatory and immune mediators[17]. This study highlights the role of the EC cell-mucosal afferent circuit as an important player in visceral pain.

Our findings add to the ever-increasing contribution of EC cells to a myriad of gut functions[11,35] such as mechano-[13,20,21] and chemo-sensation[3,9,12]. How can EC cells assume such functional diversity? The answer may reflect their location along the crypt-villus axis or within specific segments of the gastrointestinal tract[36,37] and the neuronal subtypes with which they interact, including those of vagal[12], spinal[3,38], or enteric[13] origin. Data presented here also support a role for local, rather than systemic serotonergic signaling

at the interface between EC cells and mucosal afferents, consistent with recent suggestions that primary afferent nerve fibers form synapse-like associations with enteroendocrine cells[3,12,38]. Alosetron, which is approved for the treatment of severe IBS with diarrhea in women[39], has been proposed to exert its analgesic effect centrally[40–42] or through inhibition of high threshold nociceptors within the gut wall[43]. We propose an alternative or additional mechanism to account for this sex-biased analgesic effect, namely one involving modulation of serotonergic signaling at EC cell-mucosal afferent circuits.

Irritable bowel syndrome is often initiated by infection and/or profound intestinal inflammation, but pain and hypersensitivity persist long after resolution of tissue damage[1], likely reflecting a multifactorial process involving disruption of mucosal integrity with effects on both the epithelium and underlying sensory nerve fibers. However, our results indicate that chronic activation of EC cells is, by itself, sufficient to generate persistent visceral hypersensitivity, providing a targeted experimental approach to study this maladaptive response in the absence of other confounding pathophysiologic variables. Moreover, our findings predict that EC cells represent a relevant therapeutic target for ameliorating chronic visceral pain.

Functional GI disorders are especially prevalent among women[1]. Based on our data across *in vitro*, *ex vivo*, and *in vivo* models, we speculate that EC cell-mucosal afferent signaling contributes differentially to visceral pain in female versus male mice, perhaps reflecting a greater tonic input of this pathway in females. At the same time, we consistently find that isovalerate or acute chemogenetic activation of EC cells in females fails to further increase visceral sensitivity. Thus, an enhanced EC cell-afferent circuitry may predispose females to a higher incidence of visceral pain in combination with other factors, such as estrogen[44–47]. Identifying sex-specific molecular and functional differences in EC cells may provide mechanistic insight into the well-recognized sex disparity in visceral pain syndromes. Functional GI disorders are also associated with increased anxiety, and treatment with selective serotonin reuptake inhibitors may have a dual benefit in targeting both peripheral and central sites[48,49]. Interestingly, we observed enhanced anxiety with EC cell inhibition or activation in both sexes, suggesting that this integrative behavioral state is an especially sensitive readout of visceral dysregulation, highlighting the importance of the gut-brain axis in neurogastroenterological disorders.

METHODS

Ethics

Experiments were approved and performed in accordance with the guidelines of the Animal Ethics Committees of the South Australian Health and Medical Research Institute (SAHMRI), the University of South Australia, and Flinders University, and with UCSF Institutional Animal Care Committee (IACUC) guidelines, the National Institutes of Health Guide for Care and Use of Laboratory Animals, and recommendations of the International Association for the Study of Pain. Most animals used in this study were between ten- to thirty-weeks-old and included both male and female mice. Animals were provided with ad-lib access to a standard lab diet and sterile water and housed under controlled and monitored temperature and humidity rooms with a 12h light/dark cycle.

Generation of transgenic mouse lines

Excitatory DREADD hm3Dq expression was directed to enteroendocrine cells using the Cre- and Flp-dependent hm3Dq reporter mouse, *RC::FL-hM3Dq* (Jackson Labs, Strain #026942). This mouse line was crossed with the transgenic *Pet1Flp* line[25] (gift of Dr. Susan Dymecki), which expresses Flp recombinase under the control of the ePet1 transcription factor. ePet1 is expressed in serotonergic neurons in the brain[25], and enteroendocrine cells in the intestines[50]. Mice hemizygous for *Pet1Flp* and homozygous for *RC::FL-hM3Dq* were then crossed to homozygous *Tac1Cre* (Jackson Labs, strain #021877) mice to get EC cell-specific expression of the DREADD reporter in the intestine. In addition to EC cells, a sparse population of neurons in the medullary raphe has been reported to be Tac1+/Pet+[51]. Therefore, to look at intestine-specific effects of the DREADD receptor activation in enteroendocrine cells, *Pet1Flp* hemizygous, *RC::FL-hM3Dq* homozygous mice were bred to *Vil1Cre* (Jackson Labs, Strain #021504) hemizygous, *RC::FL-hM3Dq* homozygous mice. *Vil1Cre* directs expression of Cre recombinase exclusively to the intestinal epithelium[52]. To inhibit serotonin release from EC cells, we targeted expression of the tetanus toxin light chain to enteroendocrine cells using the Cre and Flp dependent tetanus toxin light chain reporter mouse, *RC::PFTox*[24] (gift of Dr. Susan Dymecki). The same breeding scheme was deployed as above, i.e., *Pet1Flp* hemizygous/*RC::PFTox* homozygous mice x *Tac1Cre* homozygous mice and *Pet1Flp* hemizygous/*RC::PFTox* homozygous mice x *Vil1Cre* hemizygous/*RC::PFTox* homozygous mice. Of note, the above breeding schemes were required to avoid germline recombination of Cre reporter alleles by *Tac1Cre*.

In vivo assessment of pain-related behavior

We used abdominal electromyography (EMG) to monitor the visceromotor response (VMR) to colorectal distension (CRD) in fully awake animals[31,34,53]. For C57BL/6J and EC^{PFTox} experiments, the bare endings of two Teflon-coated stainless steel wires (Advent Research Materials Ltd, Oxford, UK) were sutured into the right abdominal muscle and tunneled subcutaneously to be exteriorized at the base of the neck for future access[31,34,53]. At the end of the surgery, mice received prophylactic antibiotics (C57BL/6J animals; Baytril; 5mg/kg s.c.) and analgesic (buprenorphine; 0.4 mg/10 kg s.c.), then they were housed individually and allowed to recover for at least three days before assessment of VMR. For EC^{hM3Dq} experiments, a wireless transmitter was implanted to enable repeated measurements over time (ETA-F10; Data Sciences International, New Brighton, MN USA). The transmitter was placed subcutaneously, and leads were implanted into the abdominal musculature as above. Animals were allowed to recover for at least seven days before undergoing baseline VMR. On the day of VMR assessment, mice were briefly anesthetized using isoflurane before receiving a 100 μL enema of vehicle (saline) or isovalerate (200 μM). A lubricated balloon (2 cm length) was gently introduced through the anus and inserted into the colorectum up to 0.25 cm past the anal verge. The balloon catheter was secured to the base of the tail and connected to a barostat (Isobar 3, G&J Electronics, Willowdale, Canada) for graded and pressure-controlled balloon distension. For EC^{hM3Dq} experiments, DCZ (75μg/kg I.p.) was administered 15 min prior to first distension. Where indicated, alosetron (100μg/kg s.c.) was administered 10 min prior to DCZ. Mice were allowed to recover from anesthesia in a restrainer with dorsal access for 15min prior to initiation of the distension sequence. Distensions were applied at 20–40-50–60-70–80mmHg (20 s duration each) at 2-min

intervals so that the last distension was performed ~20 min after intracolonic treatment with either vehicle or isovalerate and ~40 min of DCZ administration. Following the final distension, colonic compliance was assessed by applying graded volumes (40–200 μL, 5s duration each) to the balloon in the colorectum of fully awake mice while recording the corresponding colorectal pressure as described previously[31,34,53]. In some studies, individual animals underwent VMR to CRD assessment following intra-colonic vehicle and then isovalerate at a later time point, allowing post-vehicle and post-isovalerate VMRs to CRD to be compared within the same animal. For the VMR recordings, the EMG electrodes were relayed to a data acquisition system. The signal was recorded (NL100AK headstage), amplified (NL104), filtered (NL 125/126, Neurolog, Digitimer Ltd, bandpass 50–5000 Hz), and digitized (CED 1401, Cambridge Electronic Design (CED), Cambridge, UK) or for EC^{hM3Dq} experiments through the Ponemah Software System (Data Sciences International) for off-line analysis using Spike2 Software (CED). The analog EMG signal was rectified and integrated. To quantify the magnitude of the VMR at each distension pressure, the area under the curve (AUC) during the distension (20 s) was corrected for baseline activity (AUC pre-distension, 20 s). We also calculated the total AUC, the summation of data points across all distension pressures for each animal. VMRs were normalized to the average maximum distension VMR of control animals for each experimental group (i.e., average control VMR at 80 mmHg is 100%).

Colon-pelvic nerve preparation for flat-sheet single fiber mucosal afferent recordings

Male and female wild-type (Tac^{Cre}) or transgenic EC^{hM3Dq} or EC^{PFTox} mice were humanely killed by CO_2 inhalation. The colon and rectum with attached pelvic nerves were removed, and recordings from mucosa afferents were performed as previously described[3,22]. Briefly, the colon was removed and pinned flat, mucosal side up, in a specialized organ bath. The colonic compartment was superfused with a modified Krebs solution (in mM: 117.9 NaCl, 4.7 KCl, 25 $NaHCO_3$, 1.3 NaH_2PO_4, 1.2 $MgSO_4$ $(H_2O)_7$, 2.5 $CaCl_2$, 11.1 D-glucose), bubbled with carbogen (95% O_2, 5% CO_2) at a temperature of 34°C. All preparations contained the L-type calcium channel antagonist nifedipine (1 μM) to suppress smooth muscle activity and the prostaglandin synthesis inhibitor indomethacin (3 μM) to suppress potential inhibitory actions of endogenous prostaglandins. The pelvic nerve bundle was extended into a paraffin-filled recording compartment in which finely dissected strands were laid onto a mirror, and a single fiber placed on the platinum recording electrode. Action potentials generated by mechanical stimuli to the colon's receptive field, pass through the fibers into a differential amplifier, filtered, sampled (20 kHz) using a 1401 interface (CED, Cambridge, UK), and stored on a PC for off-line analysis. Categorization of afferents properties followed our previously published classification system[22]. Receptive fields were identified by systematically stroking the mucosal surface with a still brush to activate all subtypes of mechanoreceptors. In short, pelvic mucosal afferents respond to delicate mucosal stroking (10 mg von Frey hairs; vfh) but not circular stretch (5g). Stimulus-response functions were then constructed by assessing the total number of action potentials generated in response to mucosal stroking with 10, 200, 500, and 1000 mg vfhs. For wildtype and transgenic $EC^{PFTox\text{-}TacCre}$ mice, isovalerate (200 μM) was applied to the mucosal epithelium for 15 min via a small metal ring placed over the receptive field of interest and mechanosensitivity re-tested. For wildtype and transgenic $EC^{hM3Dq\text{-}TacCre}$ mice,

the DREADD agonist CNO (100 μM) was applied to the mucosal epithelium for 15 min via a small metal ring placed over the receptive field of interest and mechanosensitivity re-tested.

Optogenetic stimulation of colonic mucosal afferents

As *Scn10a* ($Na_V1.8$) is expressed by >95% of colonic afferents[54] but not by ECs[3], we crossed *Scn10a*-Cre mice (gift from Dr. Wendy Imlach, Monash University, Australia) with ChR2-floxed mice (JAX strain #012569; purchased from The Jackson Laboratory; Bar Harbor, ME, USA) to produce $Na_V1.8$-ChR2 mice. This allowed us to optogenetically activate colonic mucosal afferents in an EC-independent and mechano-independent manner. Colonic recordings were prepared from $Na_V1.8$-ChR2 mice using methods described above. Once mucosal afferents were identified by their responsiveness to fine mucosal stroking (10 mg vfh), but not to circular stretch (5g), afferents were left to rest for 10 minutes before optogenetic stimulation. Afferents were illuminated with a light wavelength (λ) of 470nm in 10 ms pulses at 1 Hz with intensities ranging from 0.05–34 mW using a BioLED control module (model BLS-PL04-US) coupled with a High Power Fiber-Coupled LED Light Source (model BLS-FCS-0470–10) and Multimode Fiber Patchcords (Numerical aperture: 0.37 NA, Core size: 1000 μm. Catalog # FPC-1000–37-025MA, Mightex, Pleasanton, CA 94566, US). Following baseline optogenetic stimulation, isovalerate (200 μM) was applied to the mucosal epithelium for 15 min via a small metal ring placed over the receptive field of interest before afferent sensitivity to optogenetic stimulation was re-tested. Action potentials were analyzed offline using the Spike 2 wavemark function and discriminated as single units based on a distinguishable waveform, amplitude, and duration (CED, Cambridge, UK). Optogenetic stimulation was operated by BLS-SERIES software (BLS-SA04-US).

Colon-pelvic nerve preparation and intact colon for whole nerve recordings

These experiments were performed with mice in which EC cell-selective expression of tetanus toxin or DREADD receptor was directed by *Pet1Flp;Vil1Cre* recombination. To determine the effects of intraluminal isovalerate or CNO on distension sensitive afferents, male and female wildtype (Vil^{Cre}), $EC^{hM3Dq\text{-}VilCre}$ or $EC^{PFTox\text{-}VilCre}$ mice. Preparations were like those described above for mucosal afferents; however, the preparation was kept intact, and the colon ligated at either end to allow for fluid distension (100 μL/min, 0–80mmHg). For wildtype or $EC^{hM3Dq\text{-}VilCre}$ mice, distension was performed with CNO (100 μM) applied intraluminally. For wildtype or $EC^{PFTox\text{-}VilCre}$ mice, distension was performed with isovalerate (200 μM) applied intraluminally. Whole pelvic nerve recordings were made using a sealed glass pipette containing a microelectrode (WPI, USA) attached to a Neurolog headstage (NL100AK; Digitimer, UK). Nerve activity was amplified (NL104), filtered (NL 125/126, bandpass 50–5,000 Hz, Neurolog; Digitimer, UK), and digitized (CED 1401; CED, Cambridge, UK) to a PC for offline analysis using Spike2 software (CED, Cambridge, UK). The number of action potentials crossing a pre-set threshold at twice the background electrical noise was determined per second to quantify the afferent response. Single-unit analysis was performed offline by matching individual spike waveforms through linear interpolation using Spike2 version 5.18 software. Afferent units sensitive to colonic distension were classified as Low Threshold, Wide Dynamic Range, or High Threshold based on their firing characteristics. Low threshold (LT) afferents responded below 10

mmHg of distension with afferent firing rates at 20 mmHg >20% of the maximal response. Wide Dynamic Range (WDR) afferents responded below 10 mmHg of distension with afferent firing rates at 20 mmHg <20% of the maximal response. High threshold (HT) afferents responded at distension pressures >10 mmHg.

Channelrhodopsin-eYFP expression in $Na_V1.8$-positive DRG neurons

To compare the fluorescence levels of eYFP (reporter protein to monitor channelrhodopsin expression) female and male $Na_V1.8$-ChR2 mice were humanely killed by CO_2 asphyxiation and L6 DRGs rapidly removed and placed in ice-cold PFA for 24hrs. Wild-type C57BL/6J mice were used as eYFP negative controls to set background fluorescence levels. The next day DRGs were transferred into 30% PBS sucrose/buffer for 24 hours before freezing them in OCT blocks for cryosectioning. The whole sample block was cut at 10μm thickness and serial sections were mounted on gelatin-coated slides. For imaging, slides were mounted using Prolong Diamond + DAPI (ThermoFisher Scientific). Images were taken using a 20x objective on a Leica SP8 confocal microscope at 1.72x zoom. All pictures were taken using the exact same setting. All images were saved with a 1024×1024 resolution. Sections for imaging were selected to be at least 20–30μm apart till the end of the sample. Images were analyzed using the Fiji app. Images were converted into 8-bit grey values. A threshold was set at 120 for all images, which is above C57Bl/6J negative controls. An ROI, containing only neuronal soma and no nerve fibers was selected for analysis. The mean grey value was calculated using ImageJ and plotted in Prism 9 for analysis. A two-tailed, unpaired t-test was performed to compare male versus female expression of eYFP.

Intravital GCaMP imaging of L6 DRG

Male and female mice heterozygous for *$Na_V1.8$*-Cre and GCaMP6s (Jax strain #024106; purchased from The Jackson Laboratory; Bar Harbor, ME, USA) were bred within SAHMRI's specific and opportunistic pathogen-free animal care facility. Mice were then transported to the Core Animal Facility within the University of South Australia, where all procedures took place.

Surgical procedure - —All surgical procedures, mice were anesthetized using 3% isoflurane in 100% oxygen at 2 L/min in an induction box before being transferred to a nose cone for maintenance at 1.5 – 2.5% isoflurane in 100% oxygen at 0.2 L/min. Anesthetized mice were kept on a heating pad to maintain body temperature. The surface above the region of interest was shaved and skin cleaned using alternating betadine and 70% ethanol. For the laminectomy procedure, an incision was made in the skin dorsal to the spinal region of interest, and the skin separated from the underlying muscle using spring-scissors. Using a scalpel, the fasciae of the exposed muscles were cut and retracted. Muscles were then separated from the vertebral column by blunt dissection using spring scissors, and any remaining muscle fragments were cleaned away. The dorsal laminectomy was performed by inserting the tips of small spring scissors between neighboring vertebrae, caudally to the vertebra of interest, and cutting. The transverse process was then removed, again using small spring scissors, to reveal the underlying DRG. Epaxial muscles from the left and right of the vertebral column were removed by blunt dissection to create space for the microscope objective to access the DRG. Any bleeding was controlled using gauze, cotton swabs,

and warmed saline. Mice were placed in a spinal stabilization device to reduce movement artifacts due to breathing and heartbeat. Vertebrae rostral and caudal to the exposed DRG were clamped using two sets of forceps positioned ventrally to the transverse processes and forceps clamped within the device. Mice within the stabilization device were transferred to the confocal stage for imaging and maintained under isoflurane anesthesia.

Confocal imaging and intra-colonic administration - —L6 DRGs were imaged on a Zeiss LSM710 confocal microscope equipped with both argon and helium-neon lasers. GCaMP6s fluorescence was captured using the argon laser, with excitation at 488 nm and collection at 493–556 nm. Images were captured using a Zeiss Plan-Apochromat 10x objective, 0.3 NA. Functional time-series were acquired at a rate of 0.985 frames per second, from an 850 × 850 μm region (512 × 512 pixels) using a pinhole aperture to image a slice thickness of 80 μm in the z-axis. Images were taken at baseline, following administration of 100μl boluses of either intra-colonic i) saline, ii) isovalerate (200 μM), iii) alosetron (10 μM) or iv) isovalerate (200 μM) and alosetron (10 μM) combined.

Image processing - —Drift and motion artifacts in time-lapse recordings were corrected using the motion correction module in the *EZcalcium* toolbox[55] implemented in MATLAB. Further image processing was completed using Fiji/ImageJ version 2.0.0[56]. Fluorescence traces of DRG cell bodies were extracted using custom software. Regions of interest (ROIs) were manually drawn around L6 DRG cell bodies, and their fluorescence traces were extracted as pixel averages. Baseline fluorescence (F_0) was defined as the average fluorescence during the initial four frames, and traces were calculated as the change in fluorescence normalized to baseline ($\Delta F/F_0$). Drawing of ROIs and trace extraction was performed blind to the experimental group.

In vitro Ca^{2+} imaging of DRG neurons harvested from $Na_V1.8$-GCaMP6s mice

Dorsal root ganglion neurons were isolated, spot plated on coated coverslips, and maintained at 37°C in 5% CO_2, as previously described[3]. After 24 hours in culture, coverslips were transferred to a recording chamber filled with Ringer's solution (NaCl 140 mM, KCl 5 mM, CaCl2 1.25 mM, MgCl2 1 mM, glucose 10 mM, HEPES 10 mM) at room temperature (~ 22 °C). GCaMP6S fluorescence was measured using an Olympus IX71 microscope in conjunction with a Sutter Lambda 10–3 wavelength switcher, and the Chroma filter set # 49011 (ET480/40x (Ex), T510lpxrxt (BS), ET535/50m) (Em)). Fluorescence images were obtained every 5 s, using a 10x objective with a monochrome CCD camera (Retiga ELECTRO) at 488 nm excitation. Images were taken at baseline and following administration of Capsaicin (20 nM) followed by Ringer's solution containing high K^+ (Ringer's containing 30 mM KCl). In separate experiments, images were taken at baseline and following administration of the Ca^{2+} ionophore ionomycin (5 μM). Fluorescence traces of DRG cell bodies were extracted using Metafluor software (version 7.8.0.0, Olympus). Regions of interest (ROIs) were manually drawn around neuron's cell bodies, and their fluorescence traces were extracted as pixel averages. Baseline fluorescence (F0) was defined as the average fluorescence during the initial minute, and traces were calculated as the change in fluorescence normalized to baseline (ΔF/F0). Maximum GCaMP6S fluorescence

was calculated, using Microsoft Excel, by the maximum fluorescent reached after incubation with capsaicin, high K^+ or ionomycin.

Serotonin measurements from intestinal organoids or blood

Adult male *Pet1Flp;Tac1Cre;RC::FL-hM3Dq*, *Tac1Cre;Pet1Flp;PFTox*, or *Tac1Cre* mice were used to generate intestinal organoids as previously reported[57]. Organoids were maintained in organoid growth media (advanced Dulbecco's modified Eagle's medium/F12 supplemented with penicillin/streptomycin, 10 mM HEPES, Glutamax, B27 [Thermo Fisher Scientific], 1 mM N-acetylcysteine [Sigma], 50 ng/mL murine recombinant epidermal growth factor [Thermo Fisher Scientific], R-spondin1 [10% final volume], and 100 ng/mL Noggin [Peprotech]) and were passaged every 6–7 days. For adeno-associated viral (AAV) infection of organoids, day 6–7 organoids were mechanically disrupted and re-plated into 50 μL of matrigel/AAV mixture (0.8 μL each of Cre-dependent AAV harboring tdTomato and GCaMP6s [Addgene, #28306-AAV9 and #100842-AAV9] mixed with 50 μL of matrigel [Corning]). For serotonin measurements, EC^{hM3Dq}, EC^{PFTox}, and Tac^{Cre} organoids were removed from matrigel, washed with cold DPBS + 0.1% BSA twice, and re-suspended into DPBS. Organoids were aliquoted into five tubes and incubated in 100 μL of Ringer's solution (140 mM NaCl, 5 mM KCl, 2 mM $CaCl_2$, 2 mM $MgCl_2$, 10 mM D-glucose, and 10 mM HEPES-Na [pH 7.4]), Ringer's + 50 μM allyl isothiocyanate (AITC), or Ringer's + 1.7 μM deschloroclozapine (DCZ) for 15 min. For serum serotonin measurements, mice were anesthetized with 2.5% avertin and blood was collected by cardiac puncture in microcapillary tubes (SAFE-T-FILL) with clot activator. For EC^{hM3Dq}experiments, DCZ (75 μg/kg i.p.) was administered 15 min before the blood draw. The blood was allowed clot for at least 1 hour. Serum was then collected and stored at −20 °C until further use. Serotonin levels from organoids or serum were quantified using an ELISA kit (Eagle Biosciences or LDN) and SpectraMax iD5 microplate reader (Molecular Devices).

Calcium imaging

AAV-infected organoids were mechanically dissociated 5–6 days post-infection and placed on Cell-Tak (Corning) coated coverslips in the imaging chamber containing Ringer's solution. Organoids were maintained under a constant laminar flow of Ringer's solution applied by a pressure-driven micro-perfusion system (SmartSquirt, Automate Scientific). EC cells were identified by tdTomato expression. GCaMP imaging was performed with an upright microscope equipped with an ORCA-ER camera and a Lambda LS (Sutter). GCaMP6s expression was confirmed before each measurement by applying high K^+ solution (70 mM KCl, 70 mM NaCl, 2 mM $MgCl_2$, 2 mM $CaCl_2$, 10 mM D-glucose, and 10 mM HEPES-Na [pH 7.4]), and 1.7 μM DCZ was applied when the cell responded to high K^+. $\Delta F/F_0$ was calculated after background subtraction.

Behavioral experiments

All behavioral experiments were conducted between ZT6 – ZT10. All experimental mice were transferred to the behavior testing room 45 min prior to the beginning of the behavioral tests to habituate them to testing room conditions. These experiments were performed with mice in which EC cell-selective expression of tetanus toxin or DREADD receptor was directed by *Pet1Flp*;*Tac1Cre* recombination.

Elevated plus maze (EPM) - —Mice were placed in the center of an elevated plus maze (EPM) 50 cm above the floor; the dimensions of each arm were 35 cm × 5 cm, with the closed arms having a 15 cm high wall and a center area of 5 cm × 5 cm. A mouse was placed in the center area of the maze and allowed to explore freely for 5 min. Each mouse was given one trial. The time spent and distance traveled in the open and closed arms were determined using video tracking software (ANY-maze, Stoelting, Wood Dale, IL, USA) and these measures served as an index of anxiety-like behavior. In DREADD experiments, DCZ injections (75 μg/kg) were administered intra-peritoneally for 10 mins before testing. For alosetron pre-treatment, mice were subcutaneously injected with 100μg/kg of alosetron 15 mins prior to DCZ injections.

Fear conditioning - —Behavioral sessions were conducted in the Stoelting Fear Conditioning System consisting of fear conditioning chambers connected to tone and shock generators. Stimulus presentations were controlled by the ANY-maze software. During fear acquisition on day 1, animals were acclimated to the conditioning chamber in context A for 3 minutes before exposure to four tone presentations that served as the conditioned stimulus (CS, 75 dB for 30s). Each tone presentation co-terminated with an unconditioned stimulus (US, 0.5-mA foot shock for 2s). The inter-trial interval (ITI) was set at 2 mins. On day two during the context memory test, mice were exposed to context A for 6 minutes in the absence of any tone presentations. During the fear memory test on day 3, mice were exposed to a new context (Context B) for 2 minutes followed by 4 CS presentations (with 1.5 min ITI). The % time spent freezing to context or tone was analyzed using ANY-maze software. Context A consisted of grid flooring and was cleaned with 0.02% sodium hypochlorite. Context B consisted of plexiglass flooring and was cleaned with 70% ethanol.

Marble burying - —A standard 75 in^2 cage containing clean wood chip bedding to a depth of 5 cm was prepared, with 15 marbles arranged uniformly on the surface. Mice were individually placed in the corner of the cage and the number of marbles buried (to 2/3 their depth) was counted after 30 min.

Nestlet shredding - —Mice were placed in a standard cage with a pre-weighed nestlet. Nestlets were 5 mm thick cotton fiber weighing about ~3 g. Mice were left undisturbed for 90 min. The remaining unshredded nestlet was removed and weighed to determine the percentage of nestlet material shredded.

Histology

Immunofluorescence (IF) in the small and large intestine was performed using 5 μm and 20 μm cryosections or whole-mount tissue as noted, in the brain and spinal cord using 25 μm sections, and in DRGs using whole-mount tissue. Blocking was performed with 5% w/v BSA (Sigma), 5% normal serum corresponding to secondary antibody species in 0.3% Triton-X and PBS at room temperature for 60 minutes. Primary antibodies were incubated overnight at 4°C at the indicated dilutions. Antibodies used were against serotonin (1:5000, Immunostar, 1:500 Abcam), GFP (1:500, Aves), and mCherry (1:500, Takara). Secondary antibodies from Invitrogen (Alexa Fluor 647 donkey anti-rabbit, Alexa Fluor 647 donkey anti-goat, Alexa Fluor 488 donkey anti-chicken, Alexa Fluor 564 donkey anti-rabbit) were

incubated for one hour at room temperature at 1:500 dilution. Imaging was performed on the following systems: Nikon Ti2 microscope with Crest LFOV spinning disk, Nikon Ti microscope with Yokagawa CSU22 spinning disk, and BZ-X800 Keyence fluorescence microscope. Images were assembled in ImageJ.

Gastrointestinal transit studies

Total gastrointestinal transit time was measured as previously described[58,59]. Briefly, mice were fasted overnight on wire racks with free access to water. Carmine red 6% (w/v) solution in methylcellulose was delivered by orogastric gavage (300 μL) and the time until the first red stool pellet was recorded. For colonic transit, animals were fasted overnight on wire racks with free access to water. Animals were then lightly anesthetized with isoflurane and a 3mm diameter glass bead inserted in the colon to a depth of 2 cm. The time to bead expulsion was then recorded. For EC^{hM3Dq} experiments, DCZ (75 μg/kg i.p.) was administered to both Tac^{Cre} control and hM3Dq expressing animals 15 min before the start of each study. Studies were standardized to begin ~9 A.M. local time.

Statistics, blinding, and randomization

All statistical tests are described in each figure legend, with additional details provided for all panels in Extended Data Table 1. Prior to statistical analyses, all data were first analyzed for normal distribution using Kolmogorov-Smirnov or Shapiro-Wilk tests. All behavior, GCaMP, and nerve recordings were performed by blinded experimenters, with blinding codes revealed post-analysis to allow for statistical comparisons. VMR data were normalized with the average maximal response taken as 100%. Optogenetic mucosal afferent data are expressed as the threshold for action potential activation (mW/mm^2). Unless otherwise stated, data are presented as mean ± SEM and analyzed using Prism software (version 9.50, GraphPad, San Diego, CA USA). Differences were considered statistically significant at $p < 0.05$. N = number of animals and n = number of afferents/cells/organoids. Genetically modified mice and control littermates were randomly allocated from different cages of male and female mice for analyses. Group sizes of males and females were used to achieve sufficient power for statistical significance for all measurements and after genotypes of mice were unblinded. Measurements included visceromotor responses, afferents recordings, behavioral, and in vitro and intra-vital experiments. For all experiments involving drug vs. vehicle, animal selection was randomized.

DATA AVAILABILITY STATEMENT

All data generated or analyzed during this study are included in this published article (and its supplementary information files).

Extended Data

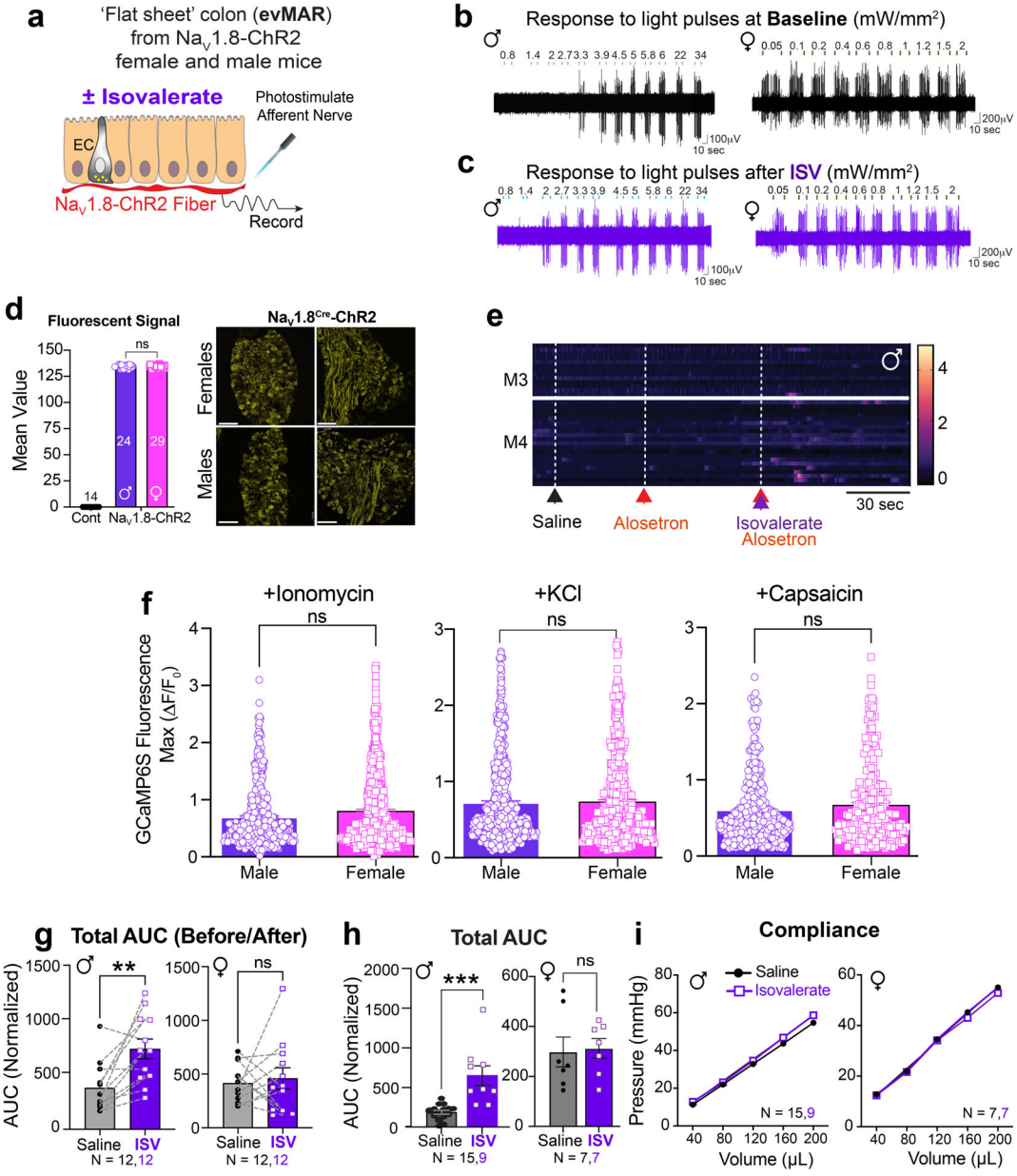

Extended Data Figure 1. Sex-specific sensitization of mucosal afferents and visceromotor responses by isovalerate.

a, Graphical scheme of *ex vivo* mucosal afferent recordings (evMAR) from Na$_V$1.8-ChR2 mice. **b-c,** Representative pelvic mucosal afferent fiber responses showing that isovalerate lowers the threshold to optogenetic activation (0.05 – 34 mW/mm^2) in males whereas females display heightened baseline sensitivity. **d**, Fluorescent channelrhodopsin-eYFP signal in L6 DRG sections from Na$_V$1.8-ChR2 mice, showing no difference between sexes. Scale bars=100µm. **e**, Heatmaps from two representative males showing *in vivo* Na$_V$1.8-GCaMP6s responses of L6 DRG neurons to intracolonic application of an isovalerate bolus (200µM) after pretreatment with alosetron (10µM). **f**, Responses of dissociated DRG

neurons from male (N=3) and female (N=3) $Na_V1.8$-GCaMP6s mice showing no sex differences in responsiveness to ionomycin 5μM (females: 514 neurons from 15 coverslips, males: 521 neurons from 18 coverslips), potassium chloride (KCl 30mM; females: 478 neurons from 11 coverslips, males: 629 neurons from 18 coverslips) or capsaicin 20nM (females: 246 neurons from 11 coverslips, males: 363 neurons from 18 coverslips). **g,** Data from individual mice showing total area under the curve for all colonic distension pressures. VMRs are significantly increased in male but not female mice following intracolonic application of isovalerate (100μl bolus of 200μM) versus vehicle; male: N=12 vehicle, N=12 isovalerate, female: N=12 vehicle, N=12 isovalerate). **h,** total AUC compared across cohorts, similarly demonstrating increased VMRs over baseline (grey) following application of isovalerate (purple) in male but not female mice (male: N=15 vehicle, N=9 isovalerate, female: N=7 vehicle, N=7 isovalerate). **i**, Colonic compliance is unchanged with isovalerate in both male and female mice. Unpaired t-test, 2-tailed in panel d, Unpaired Mann Whitney U test, 2-tailed in panels f, h, Wilcoxon matched-pairs signed-rank test 2-tailed in panel g and two-way ANOVA in panel i. **p< 0.01, ***p< 0.001, error bars represent mean ± SEM. Graphical element in panel a is licensed from BioRender.

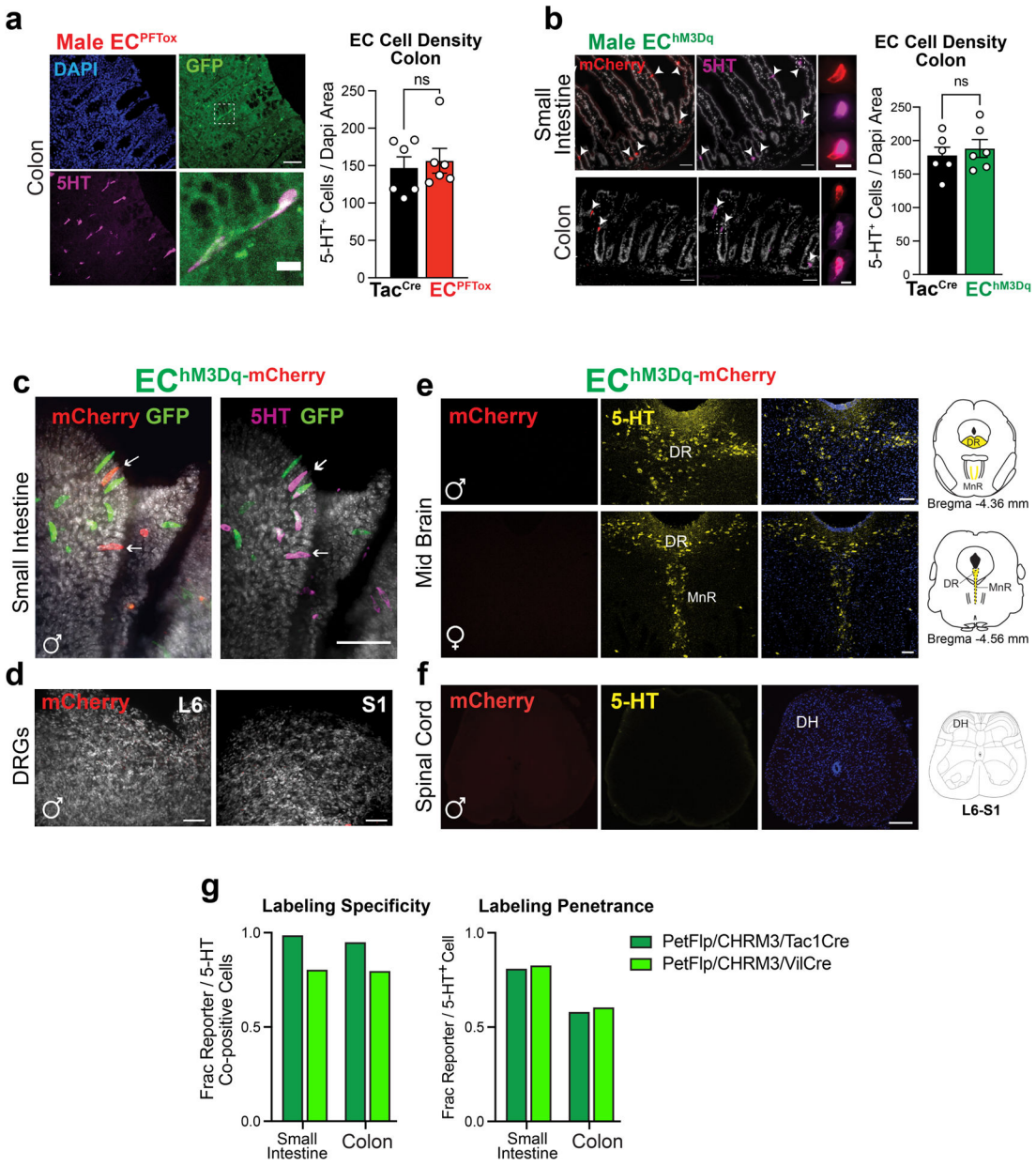

Extended Data Figure 2. Intersectional genetic strategy targets gene expression to gut EC cells.

a, Histologic sections of EC^{PFTox} (*Pet1Flp;Tac1^{Cre};RC::PFTox*) colon demonstrating colocalization of *PFTox* allele GFP reporter (green) and 5-HT (magenta); representative of 93 fields from at least 2 animals Scale bars = 50μm (upper) and 10μm (lower). Colon EC cell density is unchanged by expression of *PFTox* allele (n = 6, 6 independent fields). **b,** Histologic sections of EC^{hM3Dq} (*Pet1Flp;Tac1Cre;RC::FL-hM3Dq*) colon and duodenum demonstrating colocalization (white arrowheads) of the hM3Dq allele reporter (red) and 5-HT (magenta); representative of 129 fields from at least 2 animals. Scale bars=50μm (upper) and 10μm (lower). Colon EC cell density is unchanged following three weeks of DREADD agonist treatment (n = 6, 6 independent fields). **c,** Whole-mount small intestine (jejunum) of EC^{hM3Dq} demonstrating expression of single-(*Pet1Flp*-GFP, green)

and double-recombination (*Pet1Flp::Tac1Cre*, mCherry, red) hM3Dq allele reporters and 5HT (magenta); representative of 10 fields from at least 2 animals. Scale bar 50μm. **d,** Whole-mount DRG from spinal segments L6/S1 of EC^{hM3Dq} demonstrating the absence of mCherry (red) expression; representative of 8 fields from 1 animal. Scale bars=50μm. **e,** Images of EC^{hM3Dq} dorsal raphe (DR) and median raphe (MnR) nuclei showing 5HT-expressing neurons (yellow) and lack of mCherry (red) expression; representative of 6–8 fields from each of 3 animals. Scale bar=100μm. **f,** Images of EC^{hM3Dq} lumbosacral spinal cord (L6-S1) showing the absence of mCherry (red) and 5-HT (yellow) expression; representative of 10 fields from each of 3 animals. Scale bar=100μm. **g,** Quantitation of specificity and penetrance of intersectional genetic approach demonstrating ≥ 95% ($Tac1^{Cre}$, light grey) and 80% ($Vil1^{Cre}$, dark grey) EC cell specificity and ~60% penetrance in the colon from male mice (data collected from 20–30 random fields). Student's t-test (unpaired, 2-tailed) in panels a, b; ns = not significant, error bars represent mean ± SEM.

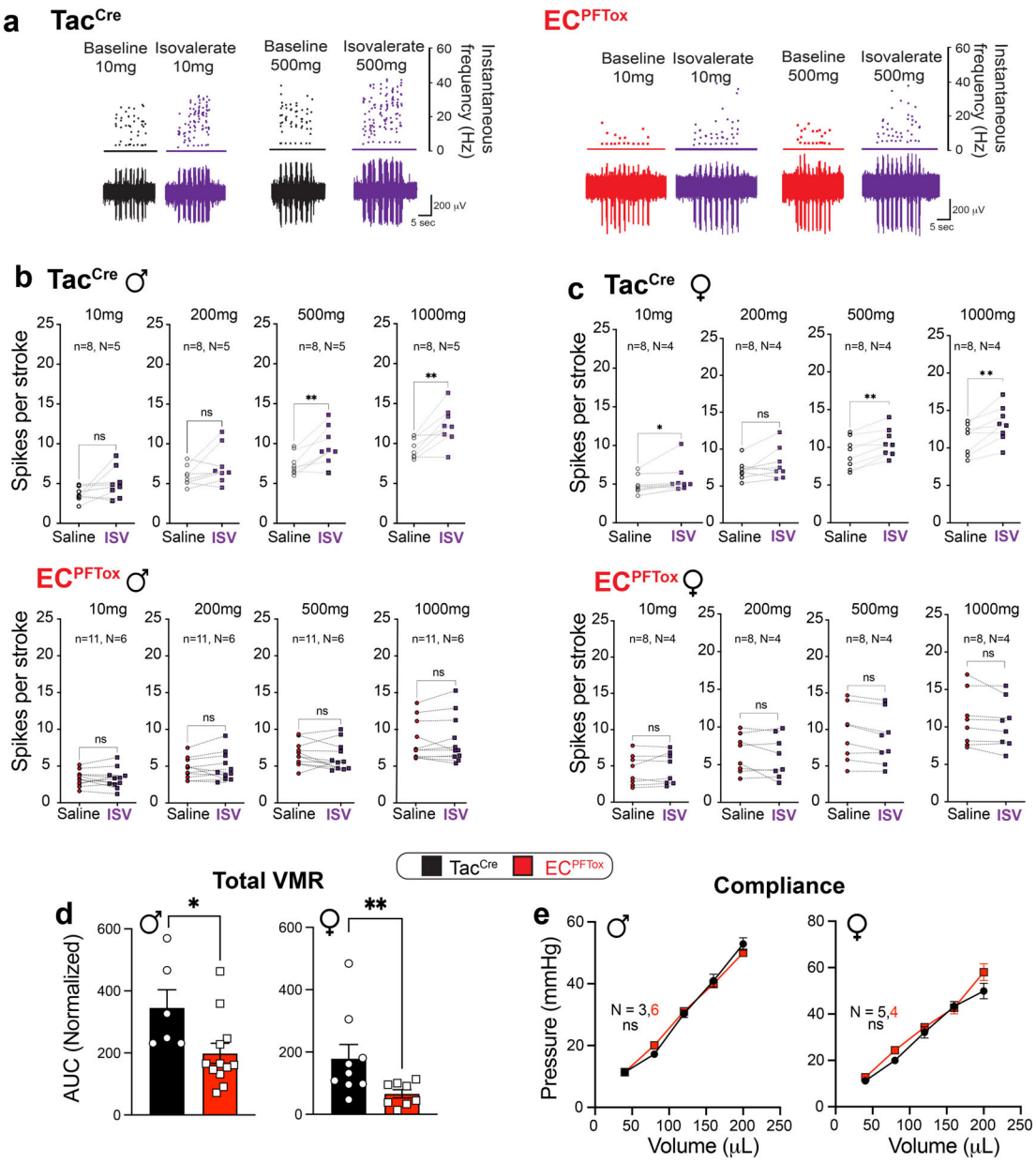

Extended Data Figure 3. Silencing EC cells attenuates responses to irritants and noxious colonic distension.

a, Representative examples of pelvic mucosal afferents firing more action potentials in response to stroking with 10 mg or 500 mg von frey hairs (vfh) in the presence of isovalerate for control (Tac^{Cre}, left panel) but not EC^{PFTox} (right panel) mice. **b,c,** Group data showing before and after isovalerate (200 μM) application response to increasing mechanical stimulation with vfh for males (**b**) and females (**c**) for control (Tac^{Cre}, upper panels) and EC^{PFTox} (lower panels) mice. **d,** Group data showing total area under the curve for all colonic distension pressures showing VMRs significantly reduced after comparing Tac^{Cre} and EC^{PFTox} males (N = 6, 12) and females (N = 9, 8). **e,** Colonic compliance is unchanged in EC^{PFTox} animals. Wilcoxon matched-pairs signed-rank 2-tailed test in panels

b, c; unpaired 2-tailed Mann Whitney U test for panel d; two-way ANOVA in panel e. *p< 0.05, **p< 0.01, ns = not significant, error bars represent mean ± SEM.

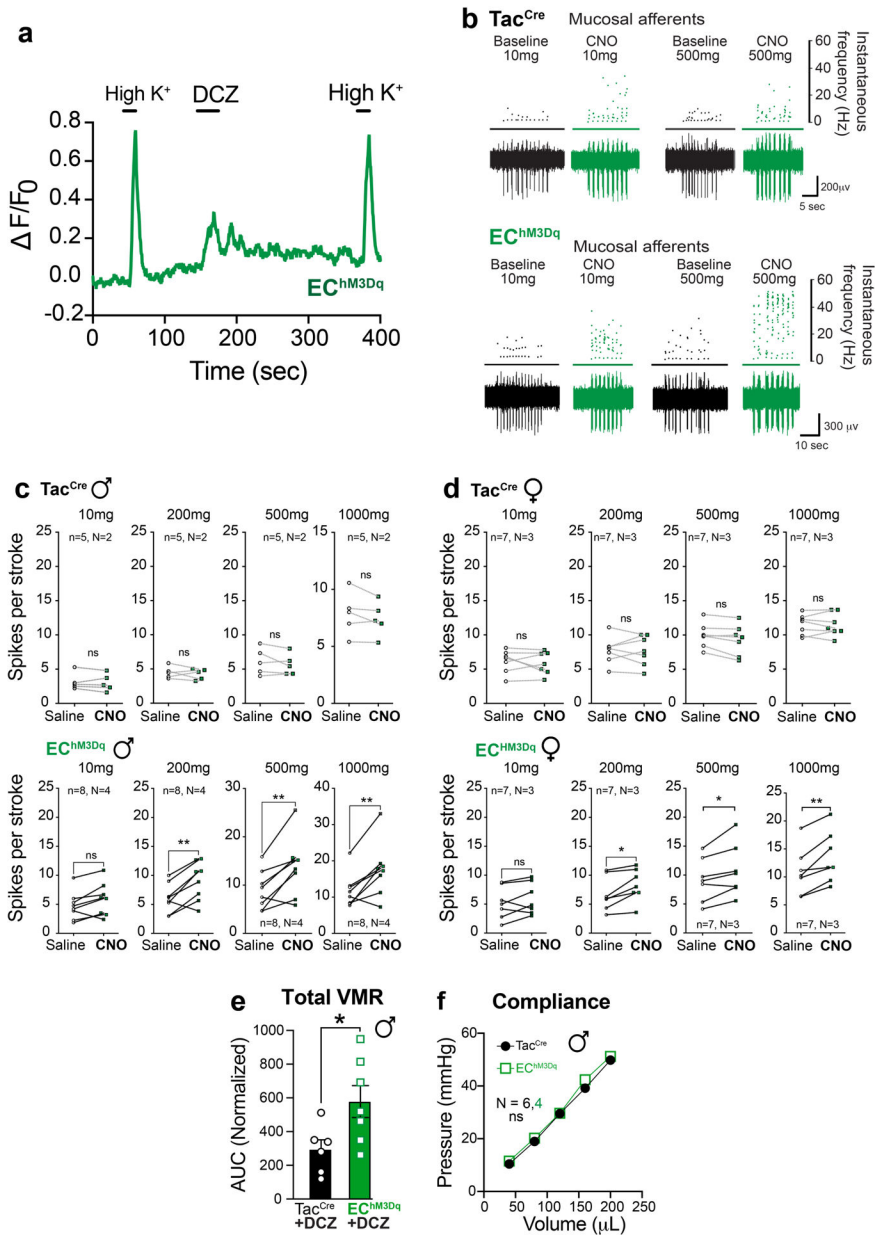

Extended Data Figure 4. Activating EC cells increases afferent output and VMR to colorectal distension.

a, DREADD agonist DCZ (1.7μM) elicits Ca^{2+} responses in EC^{hM3Dq} intestinal organoids as detected by a change in GCaMP fluorescence ratio. **b,** Representative examples of pelvic mucosal afferents firing action potentials in response to stroking with 10mg or 500mg von frey hairs (vfh) in the presence of vehicle (black/grey) or CNO (100μM; green) for control (upper panels) and EC^{hM3Dq} (lower panels) mice. **c,d,** Group data showing before and after CNO (100μM) application response to increasing mechanical stimulation with vfh for males (**c**) and females (**d**) for control (Tac^{Cre} upper panels) and EC^{hM3Dq} (lower panels) mice. **e,**

Group data showing total area under the curve for all colonic distension pressures showing VMRs significantly increased in Tac^{Cre} and EC^{hM3Dq} male mice (N = 6, 7) following DCZ (75μg/kg i.p.). **f,** Colonic compliance is unchanged in EC^{hM3Dq} animals. Wilcoxon matched-pairs signed-rank 2-tailed test in panels c, d; Student's t-test (unpaired, 2-tailed) in panel e; two-way ANOVA in panel f. *p< 0.05, **p< 0.01, ns = not significant, error bars represent mean ± SEM.

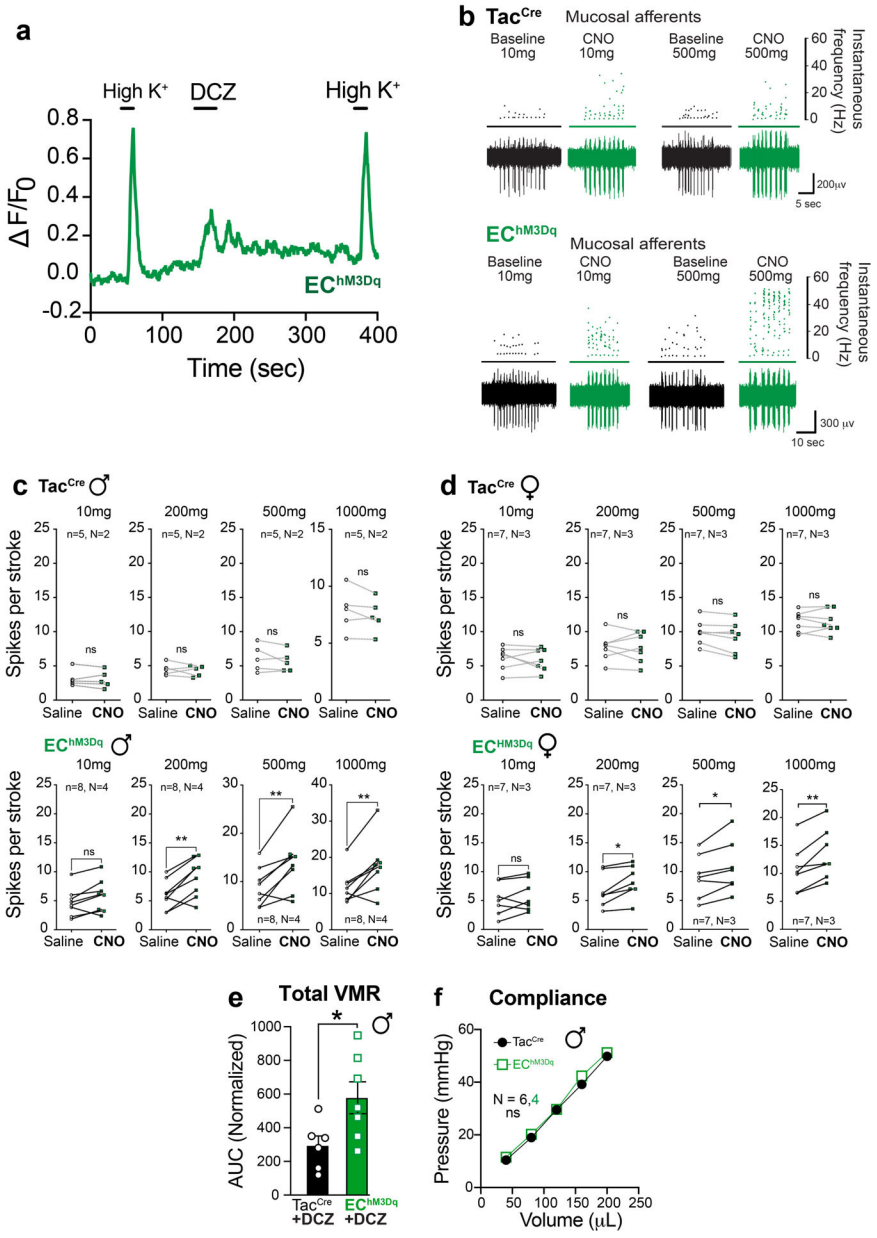

Extended Data Figure 5. Gastrointestinal transit is unchanged in EC manipulation models.

a, Total gastrointestinal and colonic transit times are similar between Tac^{Cre} control (black) and EC^{PFTox} (red) male (N = 5, 3) and female (N = 5, 4) mice. **b,** Total gastrointestinal transit times trend faster in DCZ-treated (75μg/kg) Tac^{Cre} and EC^{hM3Dq} male (N = 14, 8)

and female (N = 4, 4) mice, as did colonic transit times for male (N = 3, 4) and female (N = 7, 7) mice. Transit measurements started 15 min after DCZ i.p. injection. Unpaired 2-tailed Mann Whitney U test in panels a, b. ns = not significant.

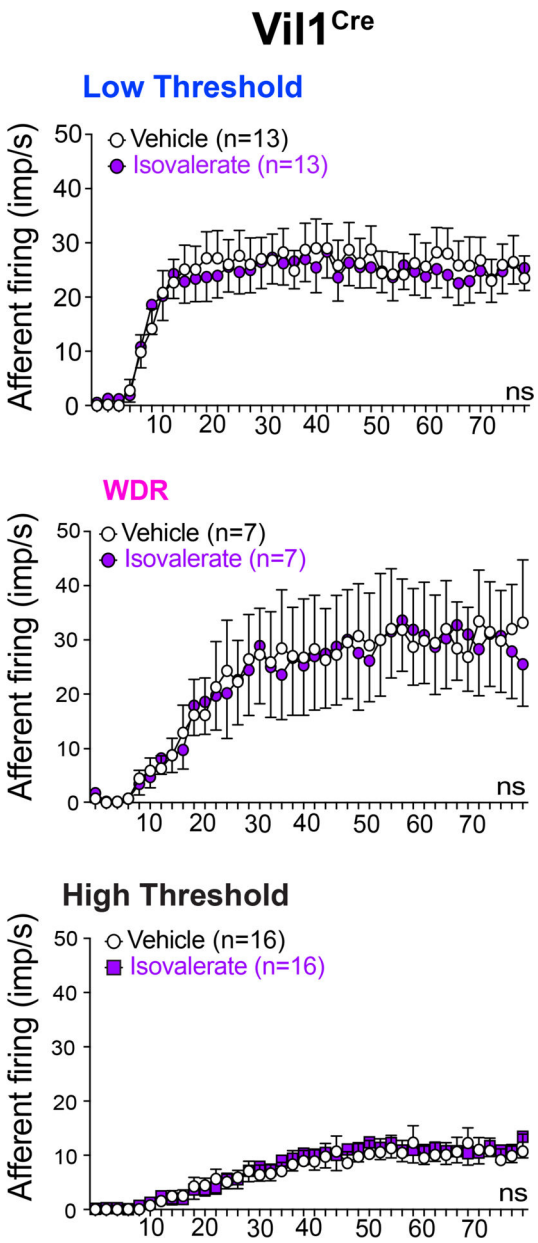

Extended Data Figure 6. EC cells do not modulate distension-sensitive afferents.

Group data showing afferent firing to increasing distension pressures in colonic preparations from Vil^{Cre} control mice at baseline and following isovalerate. Two-way ANOVA (Šidák's multiple-comparisons test); ns = not significant, error bars represent mean ± SEM.

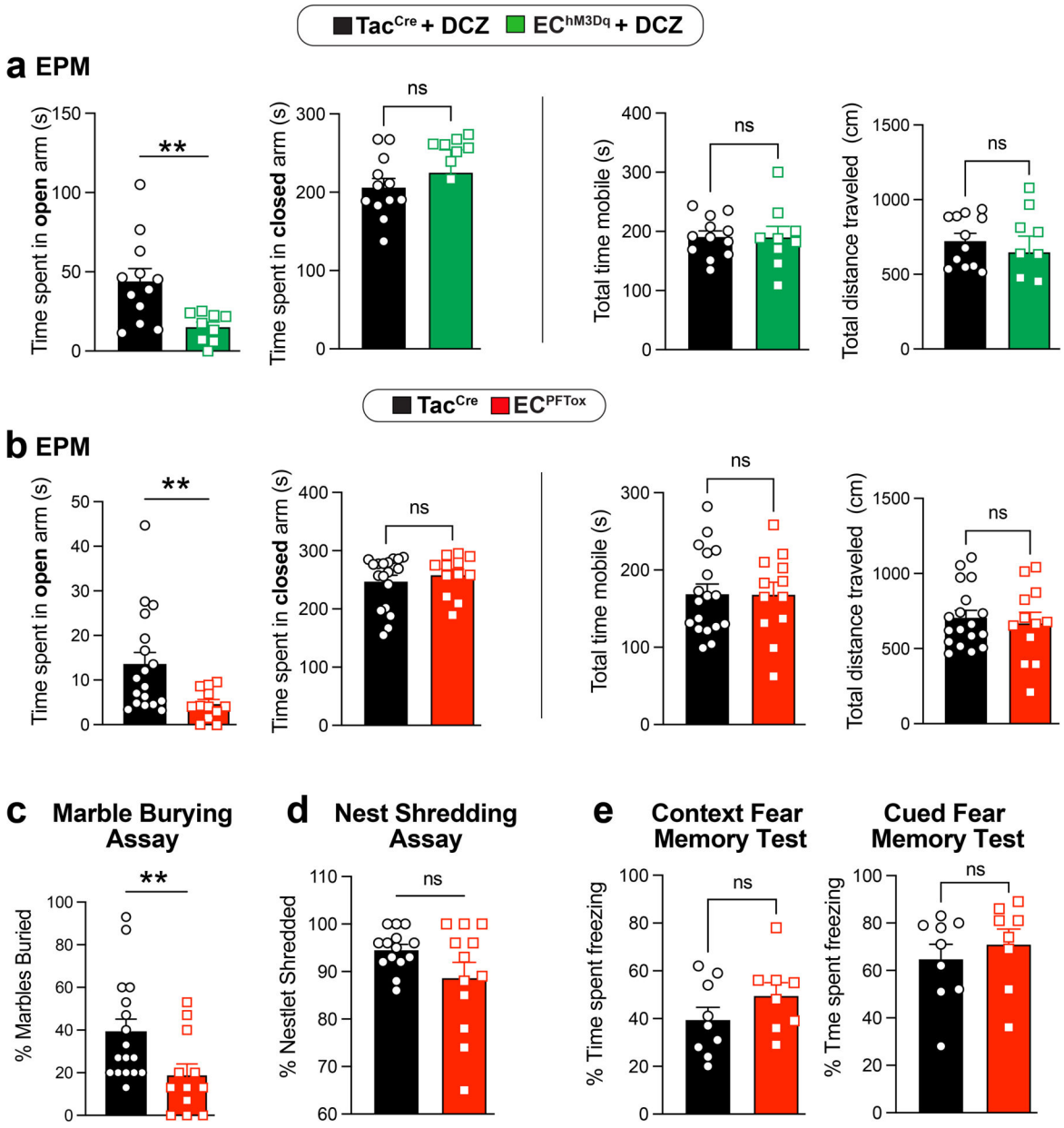

Extended Data Figure 7. Activation and silencing of EC cells in male and female mice increase anxiety-like behaviors.

a, Time spent in open or closed arms of EPM following DCZ treatment (75 μg/kg i.p.) 10 min prior to testing. The total time mobile and total distance traveled remain unchanged between Tac^{Cre}control and EC^{hM3Dq} mice (N = 12, 9). **b**, Time spent in open or closed arms of EPM for EC^{PFTox} and Tac^{Cre} control animals (N = 18, 12). The total time mobile and total distance traveled remain unchanged between $EC^{PFTox}$and Tac^{Cre} animals (N = 18, 12). **c**, EC^{PFTox} mice show significantly reduced marble-burying behavior compared to Tac^{Cre}controls (N = 17, 12). **d**, EC^{PFTox} mice do not show differences in nestlet shredding behavior (N = 14, 12). **e**, Contextual and cued fear conditioning in Tac^{Cre} and EC^{PFTox} mice (N = 9, 8). Two-way ANOVA (Šidák's multiple-comparisons test) for panel a. Unpaired

2-tailed Mann Whitney test for panels b-e. **p< 0.01, ns = not significant, error bars represent mean ± SEM.

Extended Data Table 1

List of statistical tests used and post-hoc comparisons for data shown in each panel of Figures 1 through 5.

Figure	Figure Panel	Statistical Test	Result	Post Hoc Comparison(s)	
1	**1b,** Light Intensity - Male Nav1.8-ChR2	(Left Panel): Nonlinear Regression and Chi	*(Nonlinear regression): Baseline 2.384 to*	Male Nav 1,8-ChR2 (±ISV). (Left panel): 2.0 mW/mm2 *P* <	
		squared tests. (Right panel): Wilcoxon matched-pairs signed rank 2-tailed test	*2.820, ISV 1.329 to 1.411, (Wilcoxon):* *P*=0.0010, # of Pairs = 15.	0.0001,2.7 mW/mm2 *P* =0.0047. All other stimulation intensities *NS.* (Right panel): *P*<0.001	
	lc, Light Intensity - Female Nav 1.8-ChR2	(Left Panel): Nonlinear Regression and Chi squared tests. (Right panel): Wilcoxon matched-pairs signed rank 2-tailed test	*(Nonlinear regression): unable to fit. (Wilcoxon): NS, # of Pairs = 14.*	Female Nav 1.8-ChR2 (±ISV). (Left panel): All stimulation intensities *NS.* (Right panel): *NS.*	
	lg, Male/ Female Nav 1.8-GCaMP6s Basal Activity	Unpaired, 2-tailed, Mann Whitney Utest	Male 6.870 n=67, Female 9.456 n=l 24, *P*=0.0001	Male vs. Female Nav 1.8-GCaMP6s	
	1h, Male/ Female Nav 1.8-		Male 0.9732 n=24/3545, Female 4.878 n=15/2012,*P*<0.0001		
		GCaMP6s % Neuron Basal Activity		Unpaired,2-tailed,Mann Whitney Utest	Male vs. Female Nav 1.8-GCaMP6s
	1i, Male/ Female Nav 1.8-				
		GCaMP6s %Neurons	1-Way ANOVA	$F_{(3,35)}$=6.482, *P*=0.0013	Male vs Male+Alos *P*=0.0046, Male vs Female *P*=0.0158
	Responding				
				Sidak's Multiple comparisons test: 50mmHg *P*=0.0408,	
lk, Male WT VMR AUC	2-Way RM ANOVA	Treatment effect $F_{(1,11)}$=14.97, *P*=0.0026	60mmHg *P*=0.0017,70mmHg *P*=0.0009,80mmHg *P*=0.0027 (±ISV)		
11, Female	2-Way RM ANOVA	Treatment effect	Female WT VMR AUC (±ISV). *NS* All distension pressures.		

Figure	Figure Panel	Statistical Test	Result	Post Hoc Comparison(s)
WT VMR AUC		$F_{(1,11)}$=0.1517, P=0.7045		
2	**2c**, 5 HT Release Organoids	1-Way ANOVA	$F_{(3,20)}$=94.98, P<0.0001	Male WT vs Male PFTox (±AITC) P<0.0001
	2c, Serum 5 HT Mice	1-Way ANOVA	$F_{(3,17)}$=65.04,P<0.0013	Female vs Female PFTox P=0.0130, Male vs Male PFTox P=0.0136
	2d, ev MAR Male TacCre	2-Way ANOVA	Treatment effect $F_{(1,56)}$=18.31, P<0.0001	Sidak's Multiple comparisons test: Male TacCre (±ISV) lOOOmg P=0.0147
	2d, ev MAR Females TacCre	2-Way ANOVA	Treatment effect $F_{(1,56)}$=6.825, P<0.0115	Female TacCre (±ISV) *NS*
	2d, ev MAR Male PFTox	2-Way ANOVA	Treatment effect $F_{(1,80)}$=0.0001, P<0.9909	Male PFTox (±ISV) *NS*
	2d, evMAR Females PFTox	2-Way ANOVA	Treatment effect $F_{(1,56)}$=0.2392,P<0.6267	Female PFTox (±ISV*)NS*
	2e, Male VMR AUC	2-Way ANOVA	Genotype effect $F_{(1,91)}$=16.01, P= 0.0001	TacCre vs PFTox 80mm P=0.0319
	2e, Female VMR AUC	2-Way ANOVA	Genotype effect F(1,85)=9.701, P< 0.0025	TacCre vs PFTox *NS*
	2g, Male/ Female PFTox ISV Response (%Baseline Change)	Wilcoxon matched-pairs signed rank 2-tailed test	*Male: # of Pairs = 12,12,* P=0.0210. Female: # *of Pairs = 10,11, NS*	PFTox Males/Females (+ISV).
3	**3c**, 5HT Release Organoids	1-Way ANOVA	$F_{(3,16)}$=5 .309,p=0.0099	Male WT vs Male EChM3Dq (DCZ) P<0.0085
	3c, Serum 5HTMice	1-Way ANOVA	$F_{(7,32)}$=3.522,P=0.0065	Female EChM3Dq (±DCZ) P=0.0023
	3d, evMAR Males EChM3Dq	2-Way ANOVA	Treatment effect $F_{(1,56)}$=10.77, P=0.0018	Sidak's Multiple comparisons test: EChM3Dq vs EChM3Dq+CNO 1000mg P=0.0485
	3d, evMAR Females EChM3Dq	2-Way ANOVA	Treatment effect $F_{(1,48)}$=2.856, P = 0.0975	Sidak's Multiple comparisons test: EChM3Dq vs EChM3Dq+CNO *NS*
	3e, Male VMR AUC + DCZ	2-Way ANOVA	Genotype effect $F_{(1,46)}$=17.58, P<0.0001	Sidak's Multiple comparisons test: TacCre+DCZ vs EChM3Dq+DCZ80mmHg P=0.0352
	3e, Female VMR AUC + DCZ	2-Way ANOVA	Genotype effect $F_{(1,46)}$=3.473, *P=0.*0688	Sidak's Multiple comparisons test:TacCre+DCZ vs EChM3Dq+DCZ *NS*
	3f, Male VMR AUC +ALS/DCZ	2-Way ANOVA	Genotype effect $F_{(1,90)}$=0.0171, P<0.8963	Sidak's Multiple comparisons test:TacCre (ALS+DCZ) vs

Figure	Figure Panel	Statistical Test	Result	Post Hoc Comparison(s)
				EChM3Dq (ALS+DCZ) *NS*
	3f, ISV Response Males to ALS	Wilcoxon matched-pairs signed rank 2-tailed test	*#of Pairs = 7,8, P*=0.0156	EChM3Dq (ALS+DCZ)
	3h, Male VMR AUC +DCZ 21 d	2-Way ANOVA	Genotype effect -$F_{(1,59)}$=16.30, *P*=0.0002	Sidak's Multiple comparisons test: TacCre (DCZ) vs EChM3Dq (DCZ) 80mmHg *P*=0.0352
			Treatment effect LT: $F_{(39, 234)}$ =1.189, *P*=0.2178,	
4	**4b** Afferent Firing	2-Way ANOVA	WDR: $F_{(1,480)}$ = 0.7285, *P=0.*3938, and HT: $F_{(1, 1440)}$ = 0.7072, *P=0.*4005	PFTox Males/Females (±ISV). *NS*
			Treatment effect LT: $F_{(1,1200)}$ = 0.05818,	
	4c Afferent Firing	2-Way ANOVA	*P=0.*8094, WDR: $F_{(1, 1920)}$ = 0.3484, *P*=0.5551, and HT: $F_{(1, 2160)}$ = 2.143. *P*=0.1434.	EChM3Dq Males/Females (±CNO). *NS.*
5	**5a** Distance Travelled Open Arms	Unpaired,2-tailed, Mann Whitney U test	31.50,N=12,11.60,N=9, *P*=0.0056	TacCre vs EChM3Dq Males/Females +DCZ
	5a Time Mobile Open Arms	Unpaired, 2-tailed, Mann Whitney U test	18.70,N=12,7.300, N=9, *P*= 0.0003	TacCre vs EChM3Dq Males/Females +DCZ
	5a Distance Travelled Open Arms	Unpaired,2-tailed, Mann Whitney U test	17.15,N=12,20.20,N=10, *P*=0.4461	TacCre vs EChM3Dq Males/Females +DCZ/ALS
	5a Time Mobile Open Arms	Unpaired, 2-tailed, Mann Whitney U test	9.100,N=12,10.45, N=10, *P*= 0.7581	TacCre vs EChM3Dq Males/Females + DCZ/ALS
	5b Distance Travelled Open Arms	Unpaired, 2-tailed, Mann Whitney U test	7.550,N0=18,3.550,N=12, *P*=0.0025	TacCre vs PFTOX Males/ Females
	5b Time Mobile Open Arms	Unpaired, 2-tailed, Mann Whitney U test	5.400,N=18,2.850, N=12, *P*= 0.030	TacCre vs PFTOX Males/ Females

ACKNOWLEDGMENTS

We thank Jeannie Poblete for expert assistance with animal husbandry and genotyping, the Garvan Institute, Australia for genotyping services, the Preclinical, Imaging and Research Laboratories (PIRL, SAHMRI) for the use of their small animal facility and The University of South Australia and the UCSF Nikon Imaging Core for use of their confocal imaging facilities. We thank Dr. K. Yackle and all members of our groups for many helpful suggestions and critical comments and Dr. N. Bellono for strategic contributions in the early stages of this project. We thank B. Yu for assistance in transmitter surgeries and animal care. This work was supported by NIH Training Grant T32 DK007762 and postdoctoral fellowship from the A.P. Giannini Foundation (R.D.M.) and the Damon Runyon Cancer Research Foundation (K.K.T.), a Simons Foundation Autism Research Initiative Pilot Award (514791 to D.J.), a Rainin Foundation Innovator Award (20191150 to D.J.), grants from the US National Institutes of Health (HEAL-SPARC Initiative U01NS113869 to H.A.I., D.J. and S.M.B.; R35 NS105038 to D.J.; R01 DK121657, GCRLE0320 to H.A.I., R03 DK121061 and R01 DK128346 to J.R.B.), National Health and

Medical Research Council of Australia (NHMRC) Investigator Leadership Grant (APP2008727 to S.M.B.), an NHMRC Development Grant (APP2014250 to S.M.B), an NHMRC Ideas Grant (APP1181448 to J.C.) and The Hospital Research Foundation (THRF) PhD Scholarship (SAPhD000242018 to J.M.).

REFERENCES

1. Enck P et al. Irritable bowel syndrome. Nat Rev Dis Primers 2, 16014 (2016). [PubMed: 27159638]
2. Grundy L, Erickson A & Brierley SM Visceral Pain. Annu Rev Physiol 81, 261–284 (2019). [PubMed: 30379615]
3. Bellono NW et al. Enterochromaffin Cells Are Gut Chemosensors that Couple to Sensory Neural Pathways. Cell 170, 185–198.e116 (2017). [PubMed: 28648659]
4. Racke K & Schworer H Characterization of the role of calcium and sodium channels in the stimulus secretion coupling of 5-hydroxytryptamine release from porcine enterochromaffin cells. Naunyn Schmiedebergs Arch Pharmacol 347, 1–8 (1993). [PubMed: 7680436]
5. Strege PR et al. Sodium channel NaV1.3 is important for enterochromaffin cell excitability and serotonin release. Sci Rep 7, 15650 (2017). [PubMed: 29142310]
6. Gershon MD Serotonin is a sword and a shield of the bowel: serotonin plays offense and defense. Trans Am Clin Climatol Assoc 123, 268–280 (2012). [PubMed: 23303993]
7. Koh A, De Vadder F, Kovatcheva-Datchary P & Bäckhed F From Dietary Fiber to Host Physiology: Short-Chain Fatty Acids as Key Bacterial Metabolites. Cell 165, 1332–1345 (2016). [PubMed: 27259147]
8. Farup PG, Rudi K & Hestad K Faecal short-chain fatty acids - a diagnostic biomarker for irritable bowel syndrome? BMC Gastroenterol 16, 51 (2016). [PubMed: 27121286]
9. Gribble FM & Reimann F Enteroendocrine Cells: Chemosensors in the Intestinal Epithelium. Annu Rev Physiol 78, 277–299 (2016). [PubMed: 26442437]
10. Gribble FM & Reimann F Function and mechanisms of enteroendocrine cells and gut hormones in metabolism. Nat Rev Endocrinol 15, 226–237 (2019). [PubMed: 30760847]
11. Liddle RA Neuropods. Cell Mol Gastroenterol Hepatol 7, 739–747 (2019). [PubMed: 30710726]
12. Kaelberer MM et al. A gut-brain neural circuit for nutrient sensory transduction. Science 361 (2018).
13. Treichel AJ et al. Specialized Mechanosensory Epithelial Cells in Mouse Gut Intrinsic Tactile Sensitivity. Gastroenterology (2021).
14. Nozawa K et al. TRPA1 regulates gastrointestinal motility through serotonin release from enterochromaffin cells. Proc Natl Acad Sci U S A 106, 3408–3413 (2009). [PubMed: 19211797]
15. Mawe GM & Hoffman JM Serotonin signalling in the gut--functions, dysfunctions and therapeutic targets. Nat Rev Gastroenterol Hepatol 10, 473–486 (2013). [PubMed: 23797870]
16. Osteen JD et al. Selective spider toxins reveal a role for the Nav1.1 channel in mechanical pain. Nature 534, 494–499 (2016). [PubMed: 27281198]
17. Sadeghi M et al. Contribution of membrane receptor signalling to chronic visceral pain. Int J Biochem Cell Biol 98, 10–23 (2018). [PubMed: 29477359]
18. Lu VB, Gribble FM & Reimann F Free Fatty Acid Receptors in Enteroendocrine Cells. Endocrinology 159, 2826–2835 (2018). [PubMed: 29688303]
19. Mars RAT et al. Longitudinal Multi-omics Reveals Subset-Specific Mechanisms Underlying Irritable Bowel Syndrome. Cell 182, 1460–1473.e1417 (2020). [PubMed: 32916129]
20. Alcaino C et al. A population of gut epithelial enterochromaffin cells is mechanosensitive and requires Piezo2 to convert force into serotonin release. Proc Natl Acad Sci U S A 115, E7632–e7641 (2018). [PubMed: 30037999]
21. Wang F et al. Mechanosensitive ion channel Piezo2 is important for enterochromaffin cell response to mechanical forces. J Physiol 595, 79–91 (2017). [PubMed: 27392819]
22. Brierley SM, Jones RC 3rd, Gebhart GF & Blackshaw LA Splanchnic and pelvic mechanosensory afferents signal different qualities of colonic stimuli in mice. Gastroenterology 127, 166–178 (2004). [PubMed: 15236183]

23. Daou I et al. Remote optogenetic activation and sensitization of pain pathways in freely moving mice. J Neurosci 33, 18631–18640 (2013). [PubMed: 24259584]
24. Kim JC et al. Linking genetically defined neurons to behavior through a broadly applicable silencing allele. Neuron 63, 305–315 (2009). [PubMed: 19679071]
25. Jensen P et al. Redefining the serotonergic system by genetic lineage. Nat Neurosci 11, 417–419 (2008). [PubMed: 18344997]
26. Erspamer V & Asero B Identification of enteramine, the specific hormone of the enterochromaffin cell system, as 5-hydroxytryptamine. Nature 169, 800–801 (1952).
27. Spohn SN & Mawe GM Non-conventional features of peripheral serotonin signalling - the gut and beyond. Nat Rev Gastroenterol Hepatol 14, 412–420 (2017). [PubMed: 28487547]
28. Brierley SM, Hibberd TJ & Spencer NJ Spinal Afferent Innervation of the Colon and Rectum. Front Cell Neurosci 12, 467 (2018). [PubMed: 30564102]
29. Uhlig F et al. Identification of a Quorum Sensing-Dependent Communication Pathway Mediating Bacteria-Gut-Brain Cross Talk. iScience 23, 101695 (2020). [PubMed: 33163947]
30. Makadia PA et al. Optogenetic Activation of Colon Epithelium of the Mouse Produces High-Frequency Bursting in Extrinsic Colon Afferents and Engages Visceromotor Responses. J Neurosci 38, 5788–5798 (2018). [PubMed: 29789376]
31. Grundy L et al. Chronic linaclotide treatment reduces colitis-induced neuroplasticity and reverses persistent bladder dysfunction. JCI Insight 3 (2018).
32. Najjar SA et al. Optogenetic inhibition of the colon epithelium reduces hypersensitivity in a mouse model of inflammatory bowel disease. Pain 162, 1126–1134 (2021). [PubMed: 33048854]
33. Jones RC 3rd, Xu L & Gebhart GF The mechanosensitivity of mouse colon afferent fibers and their sensitization by inflammatory mediators require transient receptor potential vanilloid 1 and acid-sensing ion channel 3. J Neurosci 25, 10981–10989 (2005). [PubMed: 16306411]
34. Castro J et al. Activation of pruritogenic TGR5, MrgprA3, and MrgprC11 on colon-innervating afferents induces visceral hypersensitivity. JCI Insight 4 (2019).
35. Fothergill LJ & Furness JB Diversity of enteroendocrine cells investigated at cellular and subcellular levels: the need for a new classification scheme. Histochem Cell Biol 150, 693–702 (2018). [PubMed: 30357510]
36. Koo A, Fothergill LJ, Kuramoto H & Furness JB 5-HT containing enteroendocrine cells characterised by morphologies, patterns of hormone co-expression, and relationships with nerve fibres in the mouse gastrointestinal tract. Histochem Cell Biol 155, 623–636 (2021). [PubMed: 33608804]
37. Lumsden AL et al. Sugar Responses of Human Enterochromaffin Cells Depend on Gut Region, Sex, and Body Mass. Nutrients 11 (2019).
38. Bohórquez DV et al. Neuroepithelial circuit formed by innervation of sensory enteroendocrine cells. J Clin Invest 125, 782–786 (2015). [PubMed: 25555217]
39. Brenner DM & Sayuk GS Current US Food and Drug Administration-Approved Pharmacologic Therapies for the Treatment of Irritable Bowel Syndrome with Diarrhea. Adv Ther 37, 83–96 (2020). [PubMed: 31707713]
40. Bradesi S et al. Dual role of 5-HT3 receptors in a rat model of delayed stress-induced visceral hyperalgesia. Pain 130, 56–65 (2007). [PubMed: 17161536]
41. Miranda A, Peles S, McLean PG & Sengupta JN Effects of the 5-HT3 receptor antagonist, alosetron, in a rat model of somatic and visceral hyperalgesia. Pain 126, 54–63 (2006). [PubMed: 16844296]
42. El-Ayache N & Galligan JJ 5-HT3 receptor signaling in serotonin transporter-knockout rats: a female sex-specific animal model of visceral hypersensitivity. Am J Physiol Gastrointest Liver Physiol 316, G132–G143 (2019). [PubMed: 30359082]
43. Hicks GA et al. Excitation of rat colonic afferent fibres by 5-HT(3) receptors. J Physiol 544, 861–869 (2002). [PubMed: 12411529]
44. Ji Y, Tang B & Traub RJ The visceromotor response to colorectal distention fluctuates with the estrous cycle in rats. Neuroscience 154, 1562–1567 (2008). [PubMed: 18550290]

45. Gustafsson JK & Greenwood-Van Meerveld B Amygdala activation by corticosterone alters visceral and somatic pain in cycling female rats. Am J Physiol Gastrointest Liver Physiol 300, G1080–1085 (2011). [PubMed: 21454447]
46. Ji Y, Murphy AZ & Traub RJ Estrogen modulates the visceromotor reflex and responses of spinal dorsal horn neurons to colorectal stimulation in the rat. J Neurosci 23, 3908–3915 (2003). [PubMed: 12736360]
47. Balasuriya GK, Hill-Yardin EL, Gershon MD & Bornstein JC A sexually dimorphic effect of cholera toxin: rapid changes in colonic motility mediated via a 5-HT3 receptor-dependent pathway in female C57Bl/6 mice. J Physiol 594, 4325–4338 (2016). [PubMed: 26990461]
48. Törnblom H & Drossman DA Psychopharmacologic Therapies for Irritable Bowel Syndrome. Gastroenterol Clin North Am 50, 655–669 (2021). [PubMed: 34304793]
49. Galligan JJ et al. Visceral hypersensitivity in female but not in male serotonin transporter knockout rats. Neurogastroenterol Motil 25, e373–381 (2013). [PubMed: 23594365]
50. Wang YC et al. The ETS oncogene family transcription factor FEV identifies serotonin-producing cells in normal and neoplastic small intestine. Endocr Relat Cancer 17, 283–291 (2010). [PubMed: 20048018]
51. Hennessy ML et al. Activity of Tachykinin1-Expressing Pet1 Raphe Neurons Modulates the Respiratory Chemoreflex. J Neurosci 37, 1807–1819 (2017). [PubMed: 28073937]
52. Madison BB et al. Cis elements of the villin gene control expression in restricted domains of the vertical (crypt) and horizontal (duodenum, cecum) axes of the intestine. J Biol Chem 277, 33275–33283 (2002). [PubMed: 12065599]
53. Salvatierra J et al. NaV1.1 inhibition can reduce visceral hypersensitivity. JCI Insight 3 (2018).
54. Hockley JRF et al. Single-cell RNAseq reveals seven classes of colonic sensory neuron. Gut 68, 633–644 (2019). [PubMed: 29483303]
55. Cantu DA et al. EZcalcium: Open-Source Toolbox for Analysis of Calcium Imaging Data. Front Neural Circuits 14, 25 (2020). [PubMed: 32499682]
56. Schindelin J et al. Fiji: an open-source platform for biological-image analysis. Nat Methods 9, 676–682 (2012). [PubMed: 22743772]
57. Sato T et al. Single Lgr5 stem cells build crypt-villus structures in vitro without a mesenchymal niche. Nature 459, 262–265 (2009). [PubMed: 19329995]
58. Becker L et al. Age-dependent shift in macrophage polarisation causes inflammation-mediated degeneration of enteric nervous system. Gut 67, 827–836 (2018). [PubMed: 28228489]
59. Li ZS, Schmauss C, Cuenca A, Ratcliffe E & Gershon MD Physiological modulation of intestinal motility by enteric dopaminergic neurons and the D2 receptor: analysis of dopamine receptor expression, location, development, and function in wild-type and knock-out mice. J Neurosci 26, 2798–2807 (2006). [PubMed: 16525059]

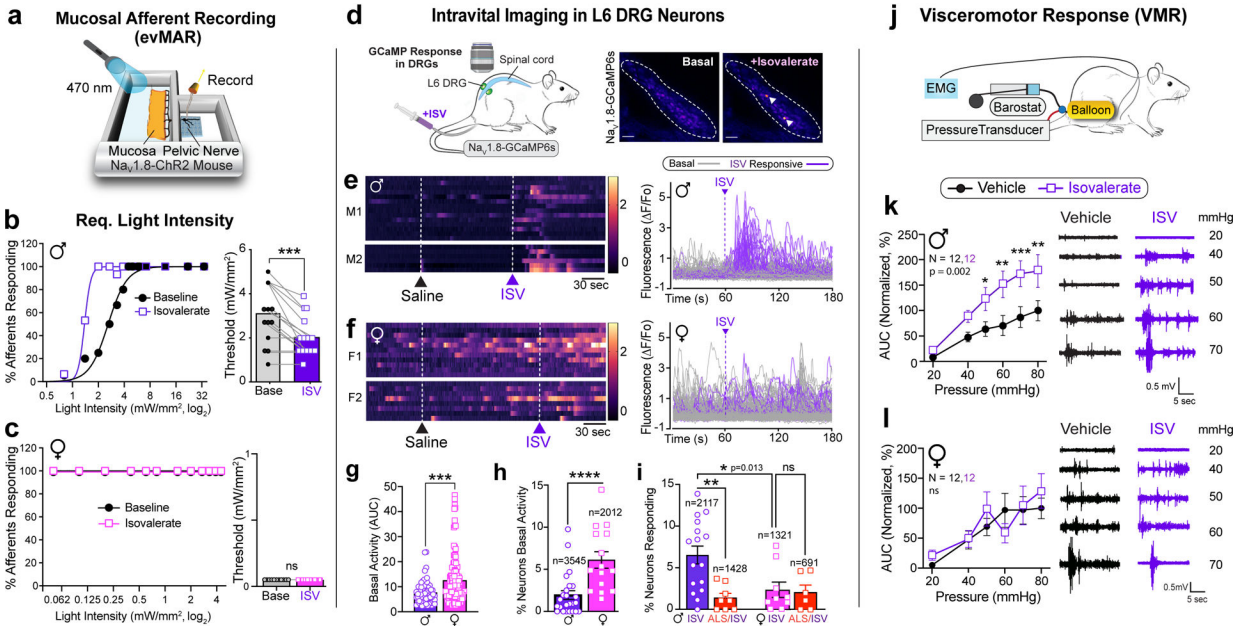

Fig. 1. EC cells mediate sex-dependent response to irritants *via* serotonergic signaling

a, Schematic of *ex vivo* 'flat sheet' colon pelvic nerve mucosal afferent recordings (evMAR) from $Na_V1.8$-ChR2 mice stimulated with 470nm light. **b-c,** Percentage of male or female afferents responding at indicated light intensities, and activation thresholds of mucosal afferents before and after isovalerate (ISV, 200μM) treatment (male: n=15; female: n=14). **d,** Illustration of intravital calcium imaging from DRGs (outlined by dashed lines) at baseline and after intracolonic delivery of isovalerate; white arrowheads indicate responsive neurons. Images are representative of data from 53 animals. Scale bars=100μm. **e-f**, Heatmaps from two representative males (e) or females (f) showing responses of L6 DRG neurons to intracolonic application of saline followed by an isovalerate bolus (200μM) with examples of fluorescence changes shown in respective righthand panels (purple traces depict isovalerate-sensitive neurons). **g**, Group data comparing magnitude of basal activity in neurons from males (n=67) and females (n=124). **h-i, P**ercentage of DRG neurons showing (h) basal activity, or (i) responses to isovalerate or isovalerate plus alosetron (ALS; 10μM) in males and females; n = total neurons analyzed per category. **j,** Experimental setup for measuring electromyography visceromotor response (VMR) of abdominal muscles to colorectal distension following intra-colonic administration of vehicle followed by isovalerate (200 μM). **k-l**, VMR responses for post-pubertal wild-type healthy males (k) or females (l). Biological replicates (N's) indicated in graphs and representative traces shown in respective righthand panels. Non-linear regression, Chi-squared, and Wilcoxon 2-tailed test in panels b, c; unpaired 2-tailed Mann Whitney test in panels g, h; one-way ANOVA in panel i, and two-way ANOVA in panels k and l (Repeated measures, Šidák's multiple-comparisons test). *p< 0.05, **p< 0.01, ***p< 0.001, ****p< 0.0001, ns = not significant, error bars represent mean ± SEM. Graphical elements in panel d are licensed from BioRender or Adobe Stock.

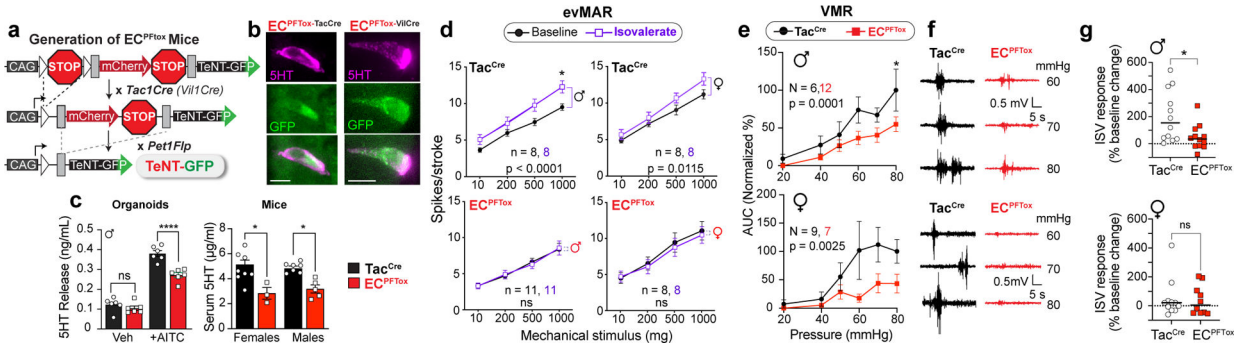

Fig. 2. Silencing EC cells attenuates colonic sensitivity to irritants and mechanical distension

a, Intersectional genetic strategy to selectively express tetanus toxin (TeNT) in EC cells. **b,** Images of EC cells showing overlapping expression of TeNT (GFP) and 5-HT (magenta); representative of >800 EC cells examined from at least 2 animals. Scale bars = 10µm. **c,** 5-HT release as detected by ELISA is blunted in EC^{PFTox} intestinal organoids compared to Tac^{Cre} controls upon stimulation with the TRPA1 agonist allyl isothiocyanate (AITC, 20µM; n = 6 or 8 organoid cultures per group) (left panel). Serum 5-HT levels from Tac^{Cre} controls and EC^{PFTox} female (N = 8, 3) and male (N = 7, 5) mice (right panel). **d,** Group data from mucosal afferent recordings (evMAR) at baseline and following isovalerate (200µM) application for Tac^{Cre} control and EC^{PFTox} male and female cohorts. **e,** VMR to colorectal distension is shown for male and female EC^{PFTox} mice compared to littermate controls. **f,** Representative traces for control Tac^{Cre} (left) or EC^{PFTox} (right) male (upper) or female (lower) mice. **g,** Percent change in total VMR for Tac^{Cre} control and EC^{PFTox} male mice (N = 12, 12) and female mice (N = 10, 11), showing loss of isovalerate sensitization in EC^{PFTox} males. One-way ANOVA in panel c; two-way ANOVA (Šidák's multiple-comparisons test) in panels c-e; Wilcoxon 2-tailed test in panel g. *p< 0.05, ****p< 0.0001, ns = not significant, error bars represent mean ± SEM.

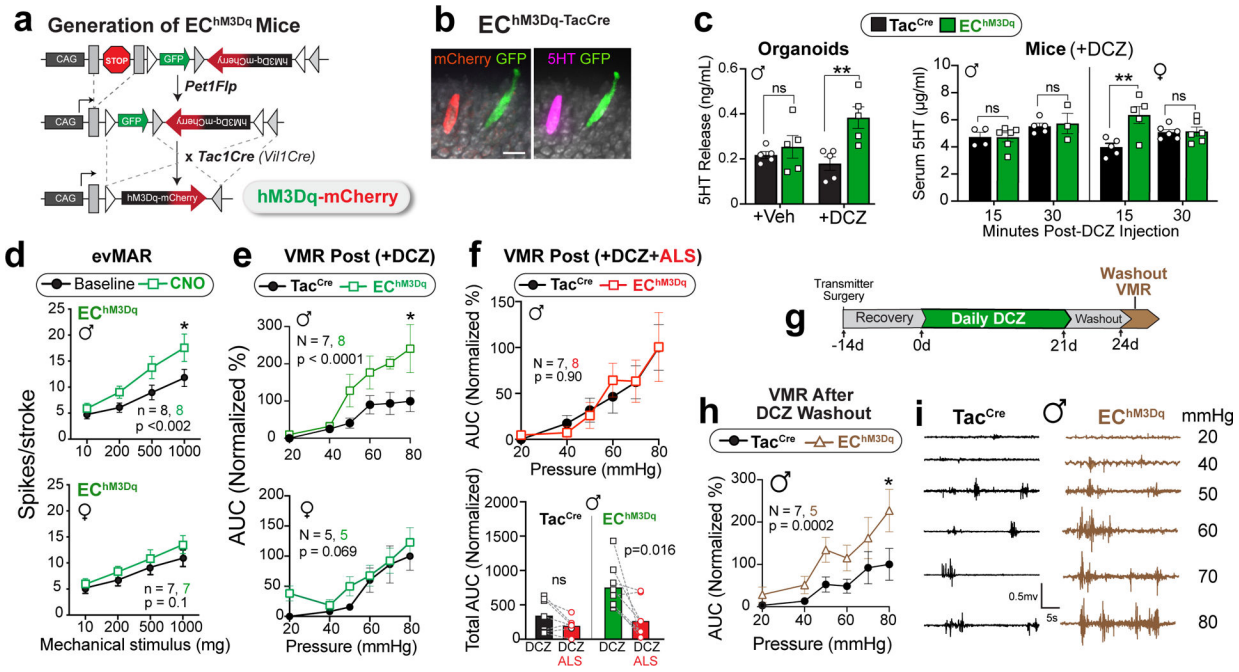

Fig. 3. Activating EC cells increases afferent output in males and induces long-term hypersensitivity

a, Intersectional genetic strategy for expressing DREADD-hM3Dq in EC cells. **b,** EC cell showing DREADD (mCherry) and 5-HT (magenta) co-expression; representative of >300 EC cells examined from at least 2 animals. Scale bar = 15μm. **c,** 5-HT release from Tac^{Cre} control or EC^{hM3Dq} intestinal organoid cultures (n = 5 per group) following treatment with DCZ (1.7μM). Serum 5-HT levels in Tac^{Cre} or EC^{hM3Dq} males at 15 min (N = 5, 6) and 30 min (N = 5, 3) and females at 15 min (N = 5, 5) and 30 min (N = 6, 6) after DCZ (75μg/kg) administration. **d,** Group data from mucosal afferent recordings (evMAR) for EC^{hM3Dq} mice at baseline and following clozapine N-oxide (CNO, 100μM) application show sensitization in males but not females. **e,** VMR data following acute stimulation with DCZ (75μg/kg, 15 min) in male (upper) and female (lower) Tac^{Cre} and EC^{hM3Dq} cohorts. **f,** Administration of alosetron (ALS; 100μg/kg) 10 min prior to DCZ (75μg/kg) prevents sensitization to colorectal distension. Individual total AUCs are shown for DCZ, and DCZ/alosetron (ALS) experiments completed one week apart in the same mice. **g,** Timeline for chronic administration of DCZ (75μg/kg) for 21 days followed by a 3-day washout. **h,** VMR data showing persistent visceral hypersensitivity in male EC^{hM3Dq} mice compared to Tac^{Cre} controls following DCZ washout. **i,** Representative traces at each distension pressure for a male Tac^{Cre} and EC^{hM3Dq} mouse. One-way ANOVA in panel c; two-way ANOVA (Šidák's multiple-comparisons test) in panels d, e, f (top) and h; Wilcoxon 2-tailed in f (lower). *p< 0.05, **p< 0.01, ns = not significant, error bars represent mean ± SEM.

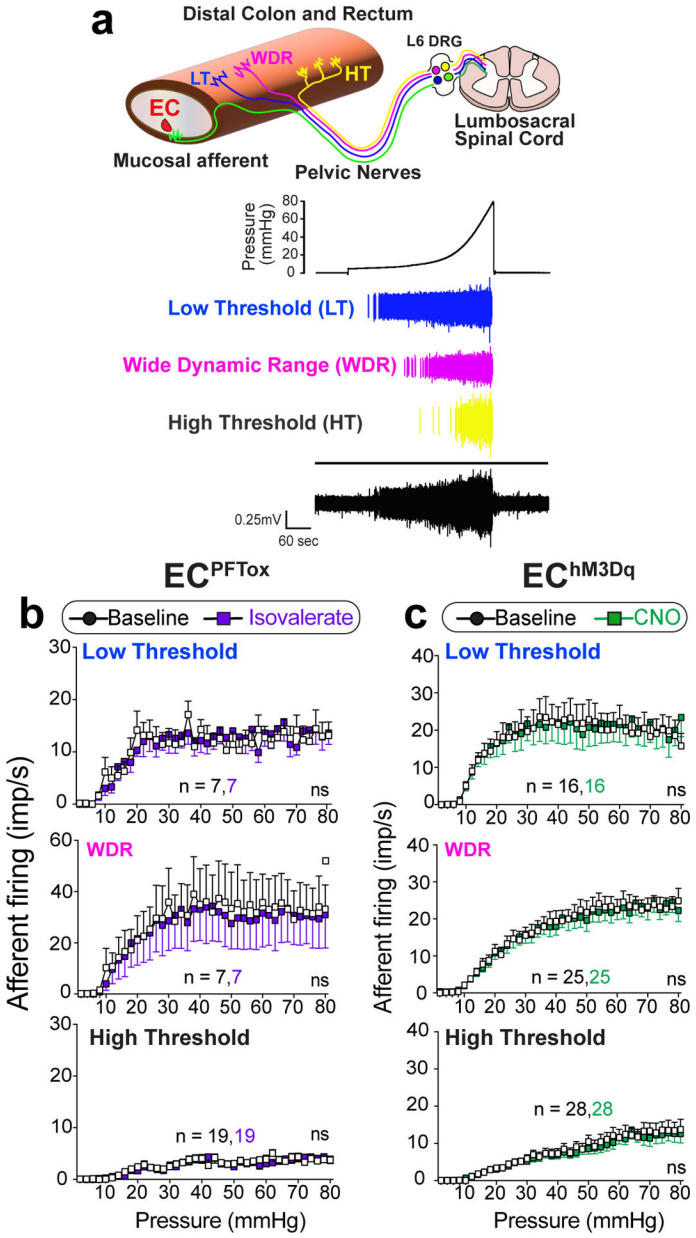

Fig. 4. EC cells do not modulate distension-sensitive afferents.

a, Graphical illustration of different afferent subtypes innervating the colon and representative *ex vivo* 'intact' colonic afferent recordings showing low threshold (LT), wide dynamic range (WDR), and high threshold (HT) distension sensitive afferents from the pelvic nerve. **b-c,** Group data showing afferent firing to increasing distension pressures in preparations from EC^{PFTox} mice (N = 3 females and 2 males combined) at baseline or following intraluminal application of isovalerate (200μM), or from EC^{hM3Dq} mice (N = 7 females and 2 males) at baseline or following intraluminal application of CNO (100μM), as indicated. Recordings were performed with mice in which EC cell-selective expression of tetanus toxin or DREADD receptor was directed by *Pet1Flp;Vil1Cre* recombination.

Two-way ANOVA (Šidák's multiple-comparisons test) for panels b, c. ns = not significant, error bars represent mean ± SEM.

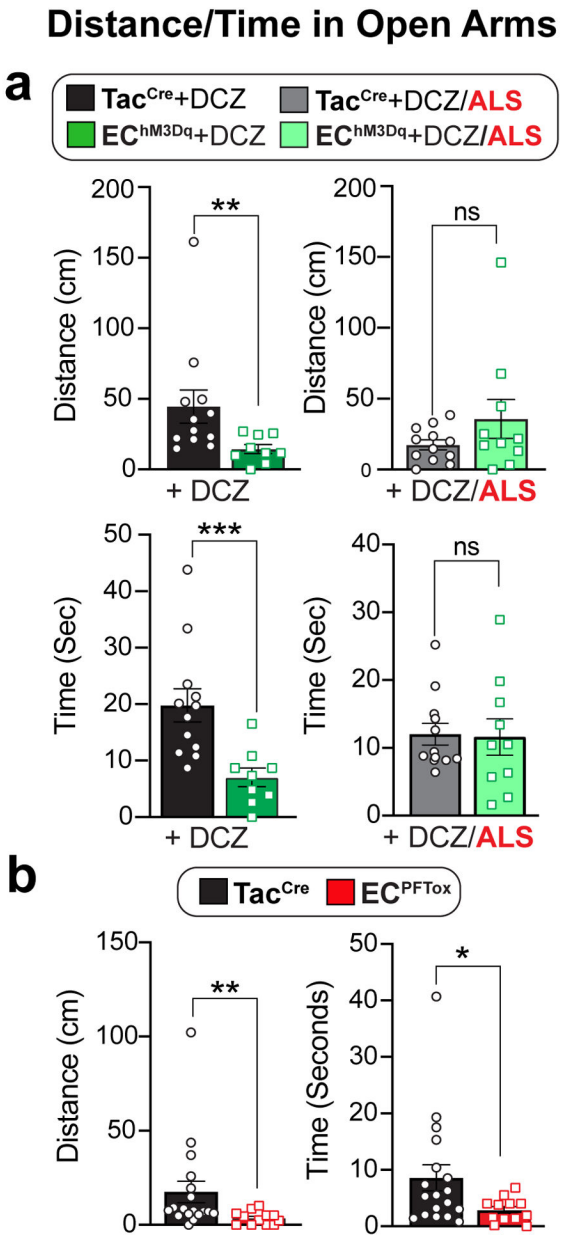

Fig. 5. Manipulating EC cell-mucosal afferent activity induces anxiety-like behavior.

Distance traveled and time mobile in open arms of an elevated plus-maze using naive male and female cohorts (combined) comparing **a,** Tac^{Cre} control and EC^{hM3Dq} mice, 10 min post-DCZ (75μg/kg, N = 12, 9) or with or without alosetron (ALS; 100μg/kg, N = 12, 10) treatment 15 min prior to DCZ administration, or **b,** comparing Tac^{Cre} to EC^{PFTox} mice (N = 18, 12). Unpaired 2-tailed Mann Whitney test for panels a, b. *p< 0.05, **p< 0.01, ***p< 0.001, ns = not significant, error bars represent mean ± SEM.